N O T I C E

THIS DOCUMENT HAS BEEN REPRODUCED FROM MICROFICHE. ALTHOUGH IT IS RECOGNIZED THAT CERTAIN PORTIONS ARE ILLEGIBLE, IT IS BEING RELEASED IN THE INTEREST OF MAKING AVAILABLE AS MUCH INFORMATION AS POSSIBLE

Optical-Communication Systems for Deep-Space Applications
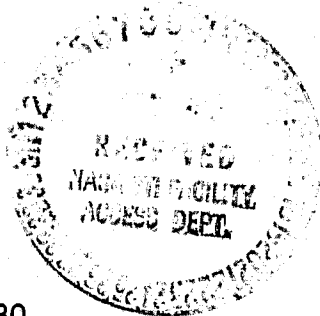
Victor A. Vilnrotter
Robert M. Gagliardi

March 15, 1980

National Aeronautics and
Space Administration

Jet Propulsion Laboratory
California Institute of Technology
Pasadena, California

Optical-Communication Systems for Deep-Space Applications

Victor A. Vilnrotter
Robert M. Gagliardi

March 15, 1980

ABSTRACT

This report examines the feasibility of using optical-communication systems for data telemetry from deep-space vehicles to Earth-based receivers. Performance analysis shows that practical, photon-counting optical systems can transmit data reliably at 30 to 40 dB higher rates than existing RF systems, or can be used to extend the communication range by 15 to 20 dB. The advantages of pulse-position modulation (PPM) formats are discussed, and photon-counting receiver structures designed for PPM decoding are described. The effects of background interference and weather on receiver performance are evaluated. Some consideration is given to tracking and beam-pointing operations, since system performance ultimately depends on the accuracy to which these operations can be carried out. An example of a tracking and pointing system utilizing an optical uplink beacon is presented, and it is shown that microradian beam pointing is within the capabilities of state-of-the-art technology. Finally, recommendations for future theoretical studies and component development programs are presented.

CONTENTS

Figures

SECTION I

INTRODUCTION

The use of optical frequencies for transmitting data from space
vehicles has been seriously considered for the past decade. Although
hardware considerations have thus far led to preference for RF and
microwave systems, advances in optical technology are rapidly making the
optical system a prime candidate for next-generation missions. The
objective of this report is to summarize the potential and feasibility
of deep-space optical data links. Primary emphasis is on discussing
practical achievable data rates, and pointing out inherent system
potentials for further improvement. Also included are discussions of
transmission formats and system models useful for optical design and
parameter trade-offs. The effort is concentrated on a deep-space-to-
Earth link model, but the results can be extended to deep-space-to-relay
satellite systems and satellite-to-satellite optical cross-links as
well.

Optical-system development up to 1970 was summarized in the
collection of articles in Reference 1-1, and many of those results are
still applicable today. Since then, more accurate theoretical models
have been developed, and the optical-communication problem has been
reexamined from several different points of view. For example,
J. R. Pierce has recently demonstrated the potential advantages of
optical systems employing photon-counting techniques, and concluded that
encoding problems, rather than thermal photons, would impose the
ultimate limit on optical-system performance (Reference 1-2). Concen-
trated efforts in optical hardware design, spurred on by developments
in fiber-optic communications, image processing, laser physics, and
the development of optical radar and ranging systems, has initiated
renewed interest in the use of optical systems for deep-space
applications.

This report presents some aspects of the optical-communication
problem applied to the deep-space environment. The discussion is
restricted to direct-detection photon-counting receivers due to the
simplicity of implementation, relative immunity from atmospheric
effects, and potential for high-rate communication offered by these
receiver structures.

SECTION II

OPTICAL-COMMUNICATION SYSTEM MODEL

Deep-space optical-communication systems can be represented in block-diagram form, as in Figure 2-1. For the interplanetary missions under consideration, the data source could represent the total output of scientific sensors and optical or microwave-imaging systems aboard a deep-space vehicle. The scientific data are modulated onto the optical carrier in a format suitable for transmission through the optical channel, and transmitted as a narrow optical beam. The optical channel consists mainly of free space, terminated by the terrestrial atmosphere in which the optical receiver is assumed to be immersed. Special-purpose subsystems must be implemented to carry out spatial acquisition, tracking, and pointing operations. Once spatial synchronization is achieved, the optical receiver collects a portion of the transmitted field, possibly corrupted by channel effects, along with thermally generated background fields. After achieving temporal synchronization, the receiver attempts to reconstruct the transmitted message, and generates an estimate of the data stream produced aboard the spacecraft. Data errors will occur due to external interference, internal noise processes, or, under the most favorable conditions, the quantum nature of the received optical field. The minimization of these errors is the main goal of receiver design.

A.   THE OPTICAL TRANSMITTER

The operation of the optical transmitter can be represented in terms of functional blocks, as in Figure 2-2. The data stream is modulated onto the optical carrier in accordance with some predetermined modulation scheme. The modulated light beam undergoes spatial processing in the optical antenna, which expands, collimates, and points the beam in the proper direction. The spatial pointing and tracking operations are carried out by a subsystem designed to track the receiver and compute the required point-ahead angles. Since point-ahead angles can be orders of magnitude greater than the transmitted beamwidth, these angles must be determined accurately at optical frequencies. The tracking and pointing operations can be aided by an optical beacon located near the receiver, while a radio-frequency uplink could also be used to update relative position and velocity information aboard the spacecraft. The angular divergence of the transmitted beam can be controlled to some extent by adjusting the internal components of the optical antenna, but the minimum beamspread is ultimately limited by diffraction effects. The diffraction-limited beam divergence, Ω_t, is a function of the optical antenna area A_t and the carrier wavelength λ. It is generally taken to be

$$\Omega_t = \lambda^2/A_t \quad \text{steradians} \tag{2-1}$$

and effectively determines the maximum achievable optical power density at the receiver. Power loss within the optical antenna can be accounted
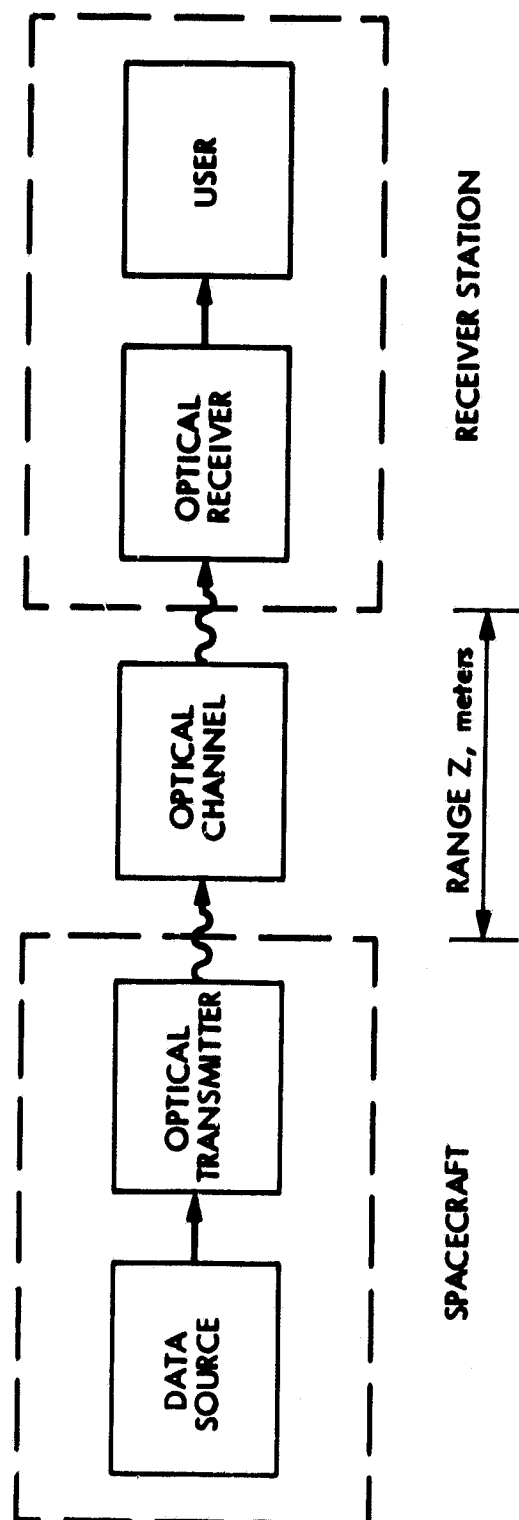
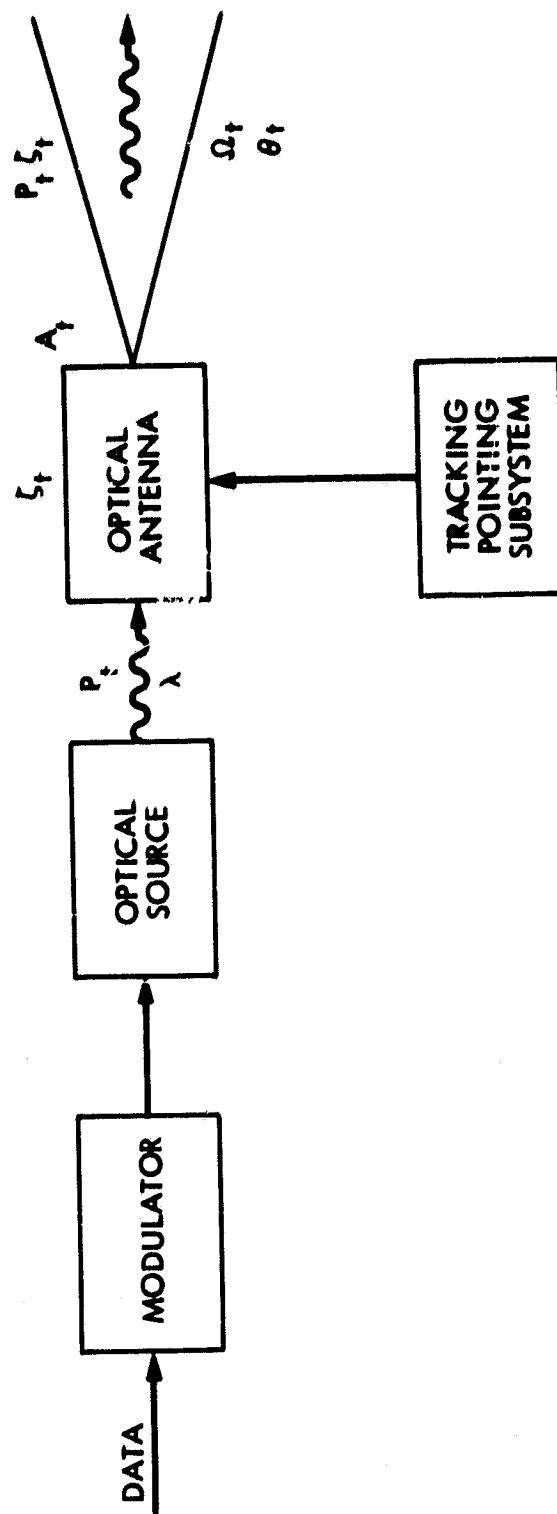Figure 2-1. Optical-Communication System Block Diagram

Figure 2-2. Optical-Transmitter Block Diagram

for by a loss factor ζ_t. Assuming P_t watts of average optical power, the far-field on-axis power density at a range of Z meters can be expressed as

$$I(Z) = \left(\frac{P_t \zeta_t}{\Omega_t}\right) \left(\frac{1}{Z^2}\right) \text{ watts/meter}^2 \qquad (2\text{-}2)$$

Equations (2-1) and (2-2) show that for fixed transmitter power P_t and wavelength λ, the on-axis power density can be increased at any range by increasing the area of the transmitter telescope. However, by so doing, we place a heavier burden on the tracking and pointing subsystems, which must aim the transmitted beam with greater accuracy. Eventually, a limit is reached where the advantages of large, diffraction-limited optics are offset by inherent pointing errors within the transmitter. The power density can also be increased by using a more powerful source, but available prime power and generally low power-conversion efficiencies limit the utility of this approach.

B.   THE OPTICAL RECEIVER

The optical photon-counting receiver consists of the functional blocks shown in Figure 2-3. The receiver could theoretically be located in Earth orbit or on the surface of the Moon, but in this report we shall assume it to be located on the surface of the Earth, at a carefully chosen site noted for extended periods of clear weather. Neglecting atmospheric weather effects (that is, assuming negligible power absorption and turbulence) and assuming arbitrarily accurate pointing and tracking at both ends of the link, the primary loss is the inverse-square reduction of received power density with distance, as shown in Equation (2-2). Figures of merit evaluated under these ideal conditions therefore represent an upper bound on achievable system performance. If the optical field is coherent over the entire receiver aperture, then an A_r square-meter optical antenna collects P_r watts of received power in a single spatial mode, where

$$P_r = A_r \, I(Z) \text{ watts} \qquad (2\text{-}3)$$

The receiver, therefore, operates as a single spatial-mode receiver, and the field-of-view Ω_r can be adjusted to its diffraction-limited value. (Receiver modes are defined as eigenfunctions of the received-field coherence kernel. The coherence function for spectrally pure fields can be expressed as the product of spatial and temporal correlation functions, hence the field modes comprise the product space of spatial and temporal eigenfunctions.) The received field can be partitioned into an average of P_r/hf photons per unit time. The optical antenna focuses the captured photons through a narrow-band optical filter onto the active surface of a photodetector, which in turn converts each
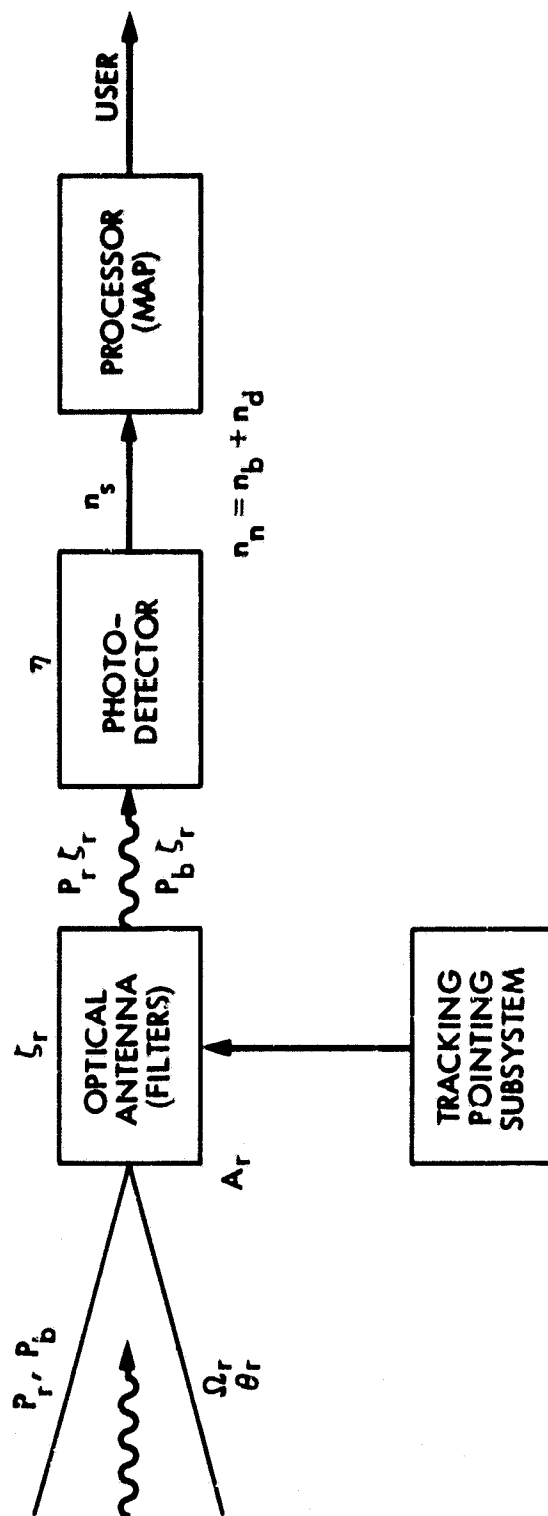
Figure 2-3. Optical-Receiver Block Diagram

photon with probability η into an electron flowing through the detector's output terminal. Accounting for antenna power loss by the factor ζ_r, and interpreting $(\zeta_r A_r \eta)$ as the effective receiver area, the effective average signal photon rate becomes

$$n_s = \frac{(\zeta_r A_r \eta)}{hf} \ I(Z) \quad \text{photons/second} \qquad (2\text{-}4)$$

where hf is the photon energy at optical frequency f, and h is Planck's constant. The post-detection processor can therefore count the effective number of photons and base its decision about the transmitted message on the observed counts. (Appropriately enough, this type of processor is called a "photon counter".)

Although single-mode reception was assumed, the receiver nevertheless captures photons from external sources within Ω_r at a rate proportional to the effective source temperature T, and proportional to the bandwidth B of the optical predetection filter. The effective average photon rate due to thermal radiation in a single spatial mode is known to be (Reference 2-1):

$$n_b = (B \eta \zeta_r)/[\exp (hf/kT) - 1] \quad \text{photons/second} \qquad (2\text{-}5)$$

These background-generated photons carry no information and serve only to impede the decoding operation. However, unless the receiver is pointed at a very hot source (such as the Sun, a bright star, or a bright planet) the number of thermally generated photons is generally negligibly small.

An additional source of interference is detector dark current, denoted by n_d. Dark current consists of electrons generated by the photodetector even in the absence of external radiation. Reducing the detector area and cooling the detector generally ameliorates this problem. Circuit noise due to resistors and recombination effects can be effectively eliminated by using photodetectors with high internal gain, as shown in Appendix A. The above noise sources can be lumped together by defining an equivalent noise count rate $n_n = n_b + n_d$. Receiver performance can then be determined by computing n_n under specific operating conditions (Section VII).

Adverse weather conditions invariable degrade the performance of single spatial-mode receivers. Atmospheric turbulence, fog, or clouds scatter and absorb the arriving signal fields, and introduce delay-dispersion effects. Receiver construction now has to be guided by the statistical properties of the received fields. The normalized field coherence function tends to approach a unit impulse under these conditions, implying that a large number of spatial modes are excited by the

received stochastic fields. Multimode reception might still be possible, perhaps at reduced rates, by processing a large number of spatial modes in the presence of background radiation (References 2-1 and 2-2), and by resorting to temporal equalization techniques when delay-dispersion effects become significant.

SECTION III

THE POTENTIAL ADVANTAGES OF OPTICAL-COMMUNICATION SYSTEMS

In this section we examine some of the advantages of optical-communication systems, and compare the performance of optical systems with their RF counterparts.

A.   OPTICAL ANTENNA GAIN

It is convenient to define the antenna gain G_t as the maximum available power density compared to that obtained with an isotropic radiator driven by the same source. Formally, this definition yields:

$$G_t = 4\pi/\Omega_t \tag{3-1}$$

Figure 3-1 shows the antenna gain as a function of antenna diameter at various wavelengths. This figure emphasizes one of the main advantages of operating in the optical regime. The extremely high antenna gain available at optical frequencies (even with modest optical antenna size) is a primary advantage of optical systems. Antenna gains on the order of 100 to 130 dB are readily obtained with half-meter-diameter optics. Similar-sized radio-frequency antennas operating at wavelengths between 1 to 100 cm can only achieve 0- to 40-dB gain and, in fact, approach the performance of isotropic radiators at the longer wavelengths. Since received power is directly related to antenna gain, the advantage of operating at optical wavelengths in a free-space channel is obvious.

B.   DATA TRANSMISSION RATE

Communication-system performance can be evaluated in terms of information transmission rate and receiver error probability. Individually, these criteria are not meaningful, since low error probabilities at low rates might be less desirable than somewhat higher error probabilities at greater transmission rates, or vice versa. However, meaningful system comparisons can be made on the basis of transmission rates at fixed error probability, or error probabilities at a given transmission rate.

It is convenient to consider the data transmission rate of an optical system as the product of the average photon information rate ρ (measured in nats/photon[1]) and the average photon rate n_s (measured in photons/second). The transmission rate R can be defined as

$$R = \rho n_s \quad \text{nats/second} \tag{3-2}$$

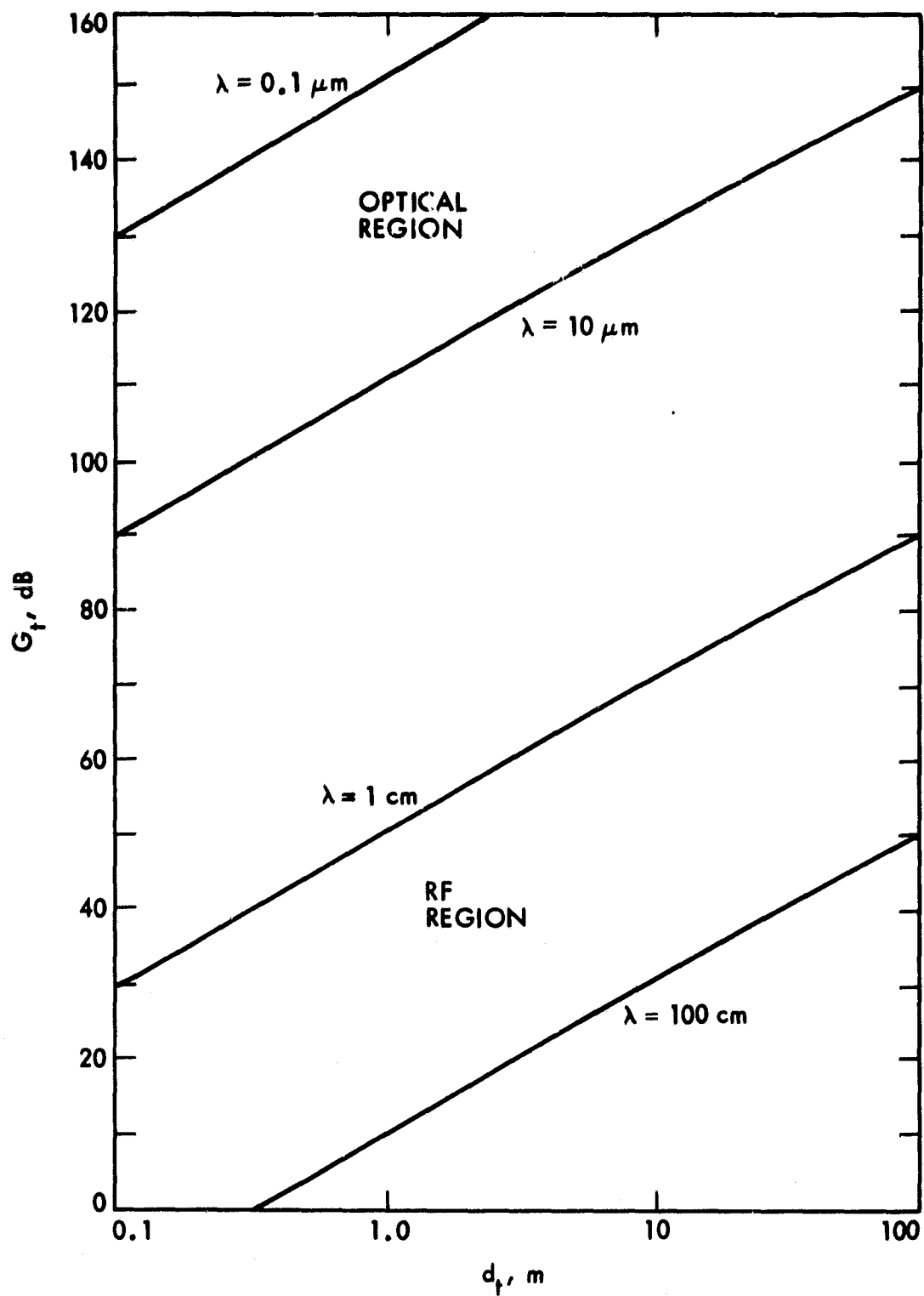[1] A "nat" is a measure of information: 1 nat = 1.44 bits.

Figure 3-1.   Antenna Gain vs Antenna Diameter

Transmission rate, therefore, depends on transmitter power, beam divergence, range, receiver aperture, and the photon information rate, which in turn depends on modulation formats and encoding schemes. It has recently been concluded that information rates greater than one nat/photon are very difficult to achieve, despite the theoretically infinite capacity of the photon channel (Reference 3-1). It is evident, however, that high photon information rates are not required to achieve high transmission rates if the photon rate can be made sufficiently great.

The average photon rate normalized to unit effective receiver area is shown as a function of range Z and field-of-view Ω_t in Figure 3-2 (for unit source power operating at $\lambda = 1$ μm) assuming perfect pointing and tracking and favorable weather conditions. Note that small beam divergence is very desirable for increasing the normalized photon rate, suggesting the use of large, diffraction-limited optics at short wavelengths. Practical considerations such as size and weight tend to limit transmitter antenna diameters to values near one meter, implying that beam divergence on the order of 10^{-12} sr should be feasible. (This conclusion is also in agreement with predicted present-day tracking and pointing capabilities, as discussed in Section VI.)

The effective receiver area $A_r \zeta_r \eta$ is obviously another important system parameter, since the photon rate depends directly on its value. Large photon buckets with collecting areas on the order of 100 m^2 can be realistically constructed using segmented optics, with 10 to 100 μrad fields-of-view (Reference 3-2). Smaller, roughly 10 m^2 collecting optics with diffraction-limited fields-of-view are also available in the form of large astronomical telescopes. The receiver loss-factor is roughly $\zeta_r \simeq 0.8$ when coated optics and reasonably wideband filters are used, while the quantum efficiency typically takes on the values $0.1 < \eta < 0.9$, depending on wavelength and detector construction. Due to relatively low laser efficiencies, average transmitted power levels on the order of 1 to 10 W can be achieved if 10 to 100 W of prime power are available. Figure 3-3 shows the variation of n_s with transmitted power $\zeta_t P_t$ and effective area $A_r \zeta_r \eta$ from a range of 10^{12} m (which corresponds roughly to the mean distance to Jupiter). The shaded parallelogram represents combinations of transmitted power and effective receiver area attainable with present-day technology. Note that photon-rates of roughly 10^8 photons/s can be achieved with reasonable laser-power receiver-area combinations, while photon rates as high as 10^9 to 10^{10} photons/s can be obtained with very large effective receiver areas, powerful lasers, and large transmitting optics.

The information rate ρ depends on the modulation format. The advantages of M-ary PPM (pulse-position modulation) formats have been demonstrated in previous studies (Reference 2-1). PPM encoding is well suited to available laser modulation techniques, requires low average power, achieves reasonably high values of ρ and is relatively immune to background interference. For these reasons, we shall be considering
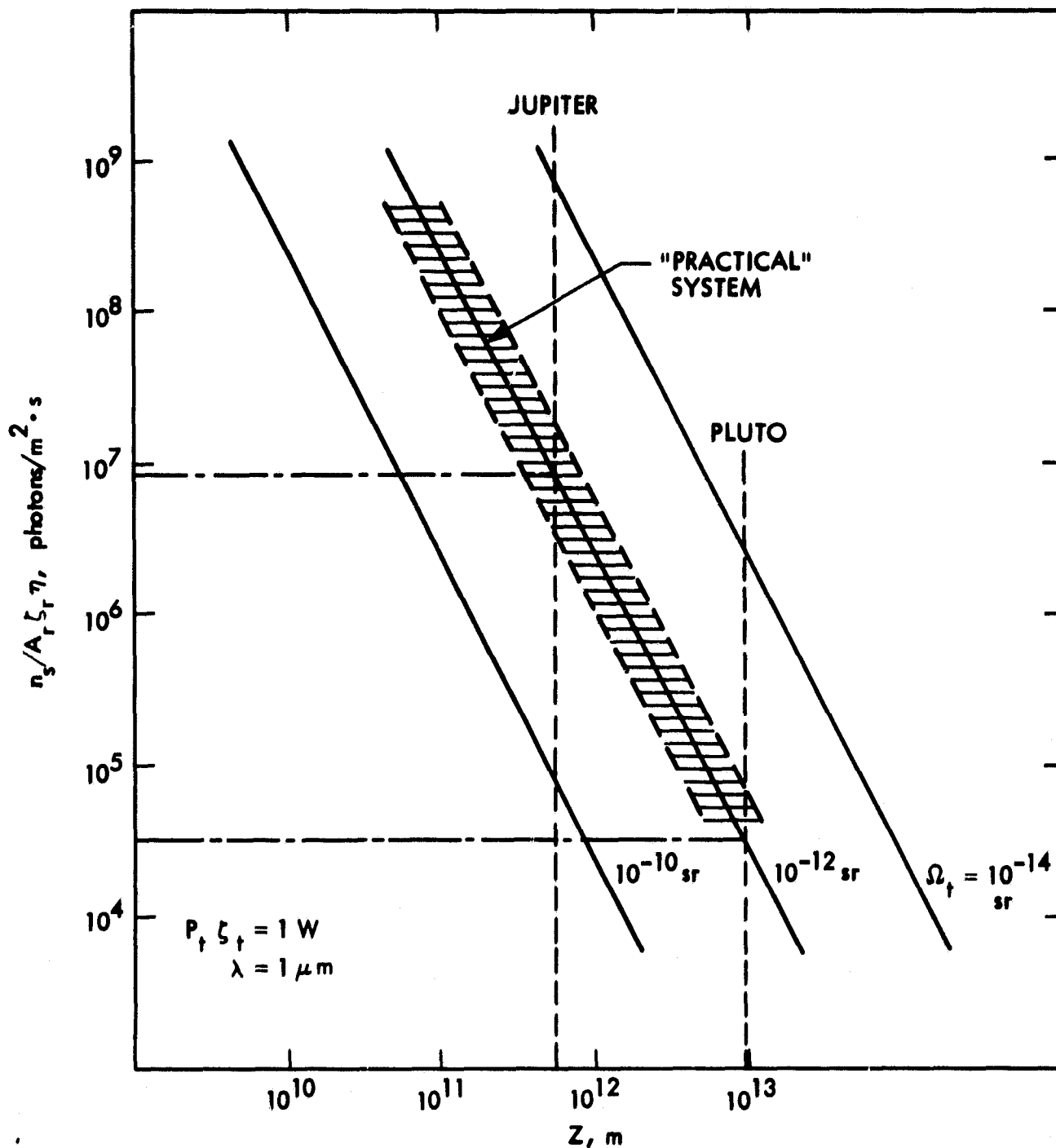
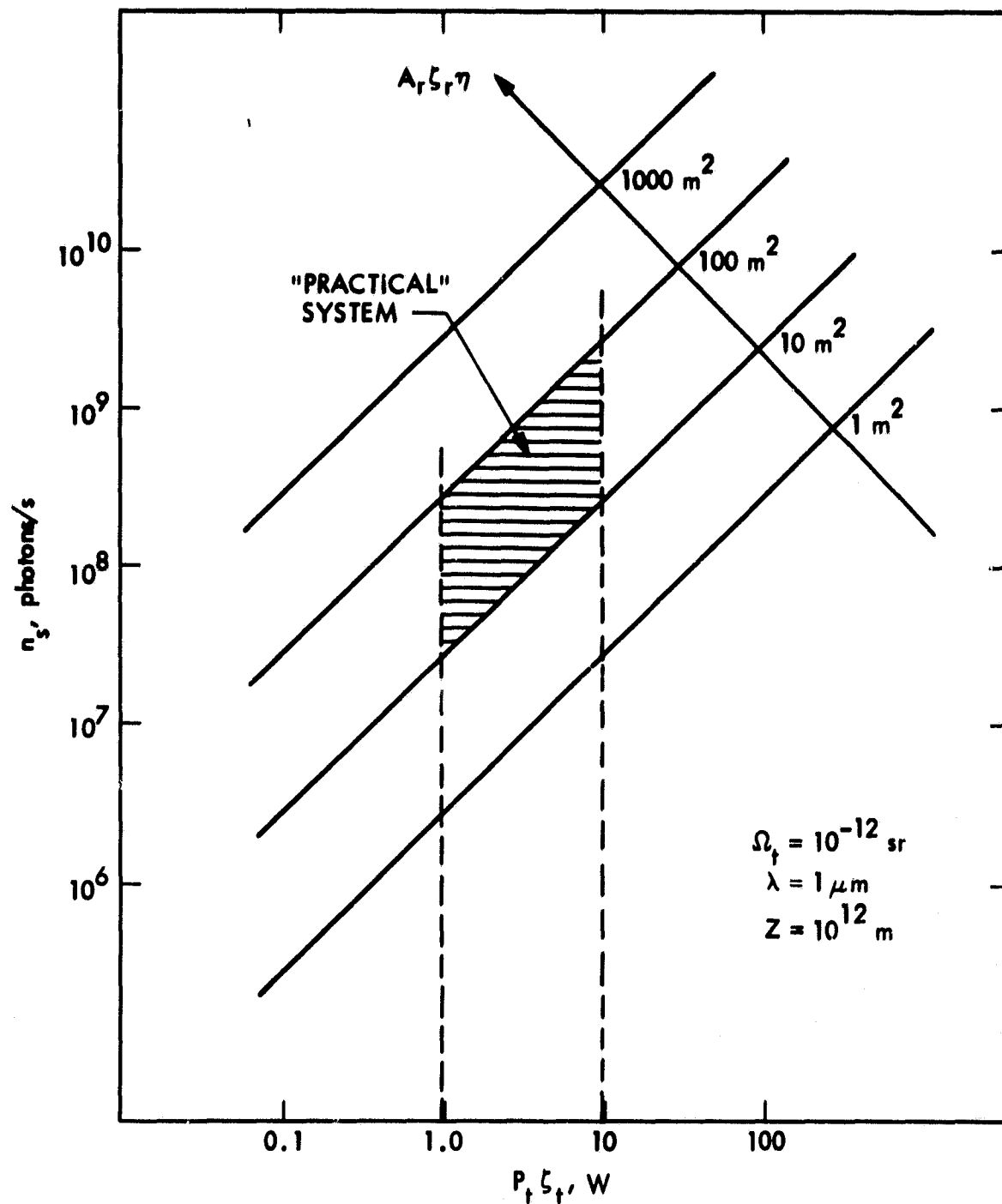Figure 3-2. Normalized Received Photon-Rate vs Distance and Beam Divergence

Figure 3-3. Photon-Rate as a Function of Source Power and Receiver Area

only PPM modulation formats in this report. (A full description of the properties of M-ary PPM signal sets is given in Section V.) It is sufficient to note here that M-ary PPM signal sets consist of M symbols, each T seconds long. Each symbol requires an average of $K_s = n_s T$ photoelectrons to transmit $\log_e M$ nats of information with erasure probability $\exp[-K_s]$. With MAP (maximum a-posteriori) decoding, the symbol error probability becomes $PSE = [(M-1)/M] \exp[-K_s]$ while the equivalent bit error probability is $PE = (1/2) \exp(-K_s)$. These error probabilities are exactly valid only in the absence of interference, but remain very good approximations until severe background interference is encountered (Appendix B). The symbol error-probability PSE has been computed for several values of M as a function of ρ, graphs of which are shown in Figure 3-4.

If a reasonable error probability is selected ($PSE \approx 10^{-5}$), it is clear that values of ρ much greater than 1 nat/photon become difficult to implement due to the extremely large values of M required. We conclude, therefore, that values of ρ much greater than 1 nat/photon cannot be conveniently implemented with PPM signal sets without incurring severe penalties in terms of system complexity.

Since the transmission-rate is the product of photon rate n_s and information rate ρ, it can be displayed parametrically as in Figure 3-5 which shows the normalized transmission rate $R/A_r \zeta_r \eta$ as a function of Z for various ρ. Note that with practical modulation schemes (such as PPM) designed to operate reliably at $0.1 < \rho < 1$, $R/A_r \zeta_r \eta$ takes on values of 3×10^6 nats/s $\cdot$ m^2 per transmitted watt at the distance of Jupiter, and degrades at the rate of 20 dB/decade with increasing distance.

C.   ACHIEVABLE TRANSMISSION RATES

The results of the previous sections can now be combined to estimate the potential transmission rates of optical systems. The receiver is assumed to consist of a large photon bucket with parameters $d_r = 10$ m, $\zeta_r = 0.8$ and $\eta = 0.2$ (photomultipliers with 20% quantum-efficiency operating near 1 μm are off-the-shelf items today). Trans-mitted average power levels of $P_t = 1$ to 10 W are assumed with $\theta_t = 10^{-6}$ rad beam divergence, and loss factor $\zeta_t = 0.8$. If coding schemes with information rates of $\rho \approx 1$ nat/photon are assumed, then the data-transmission rates shown in Figure 3-6 are obtained. The capabilities of a high-performance RF-link are included for comparison. While these results apply to clear-weather operation with negligible background interference, it is shown in Appendix B that background radiation can generally be ignored for orbiting receivers, and that even for terrestrial receivers background noise becomes significant only under unusual circumstances.
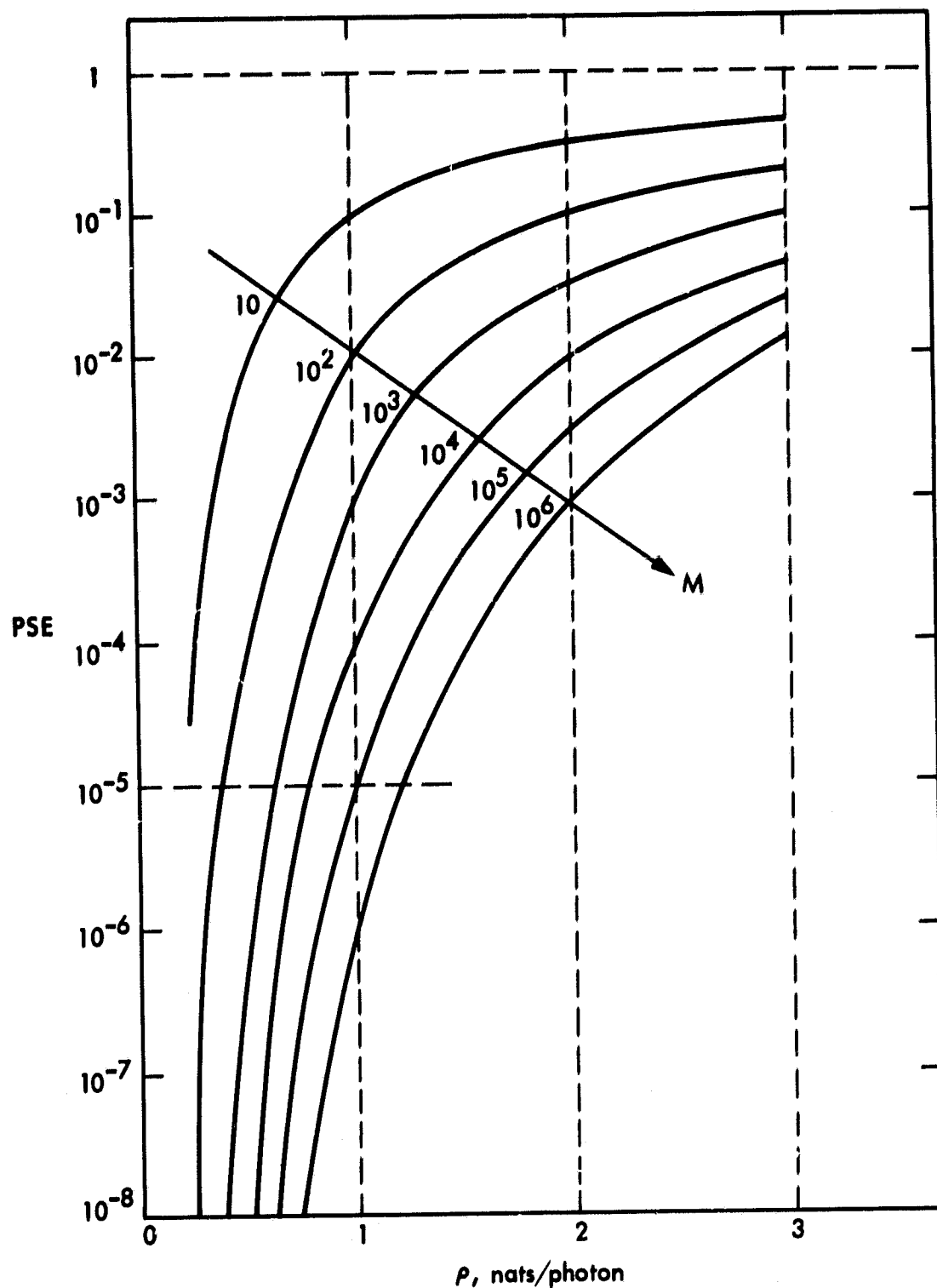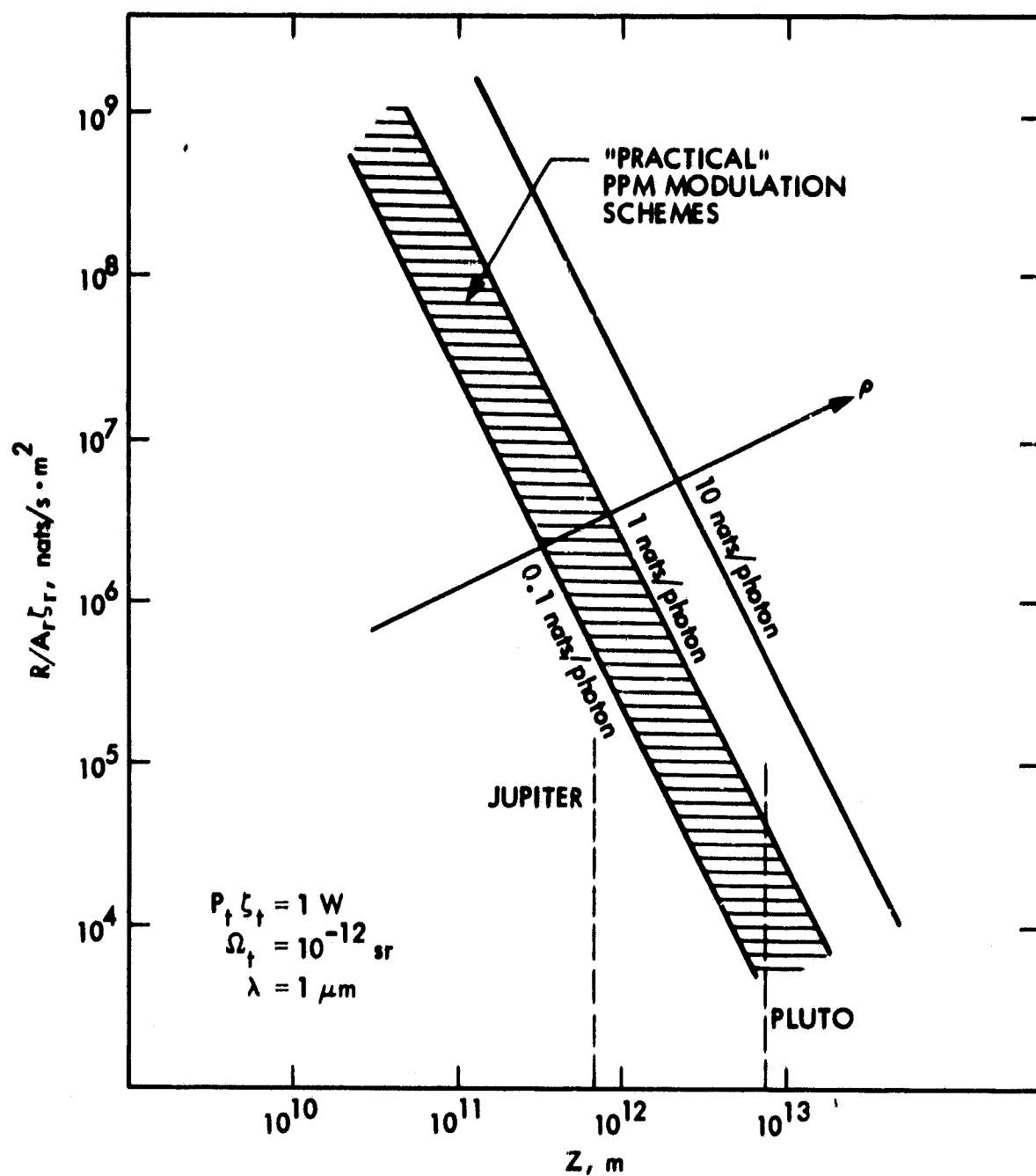
Figure 3-4. PSE vs ρ for M-ary PPM Signal Sets

Figure 3-5. Normalized Data Rate as a Function of Range and
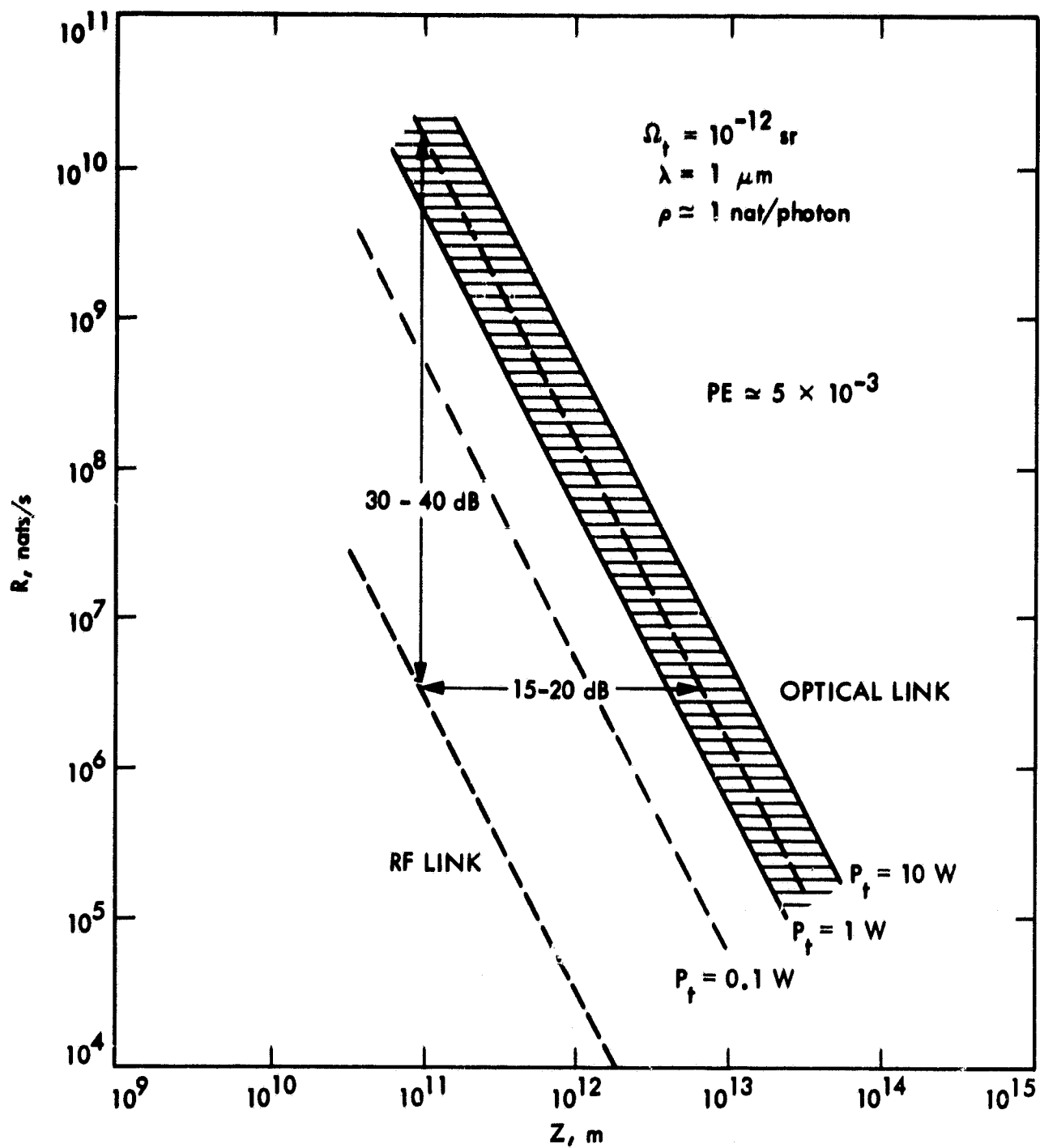Information Rate

Figure 3-6. Achievable Data Rates for Optical and RF Systems

In Figure 3-6, we compare the transmissions rate of a hypothetical PPM-modulated optical telemetry system operating at transmitter power levels of 1 to 10 W with that of the Voyager-Goldstone microwave link. Both systems are assumed to be operating at a bit-error probability of $PE = 5 \times 10^{-3}$ (or $PSE = 10^{-2}$ for the optical MAP system) (Reference 3-3) corresponding to Voyager imaging data requirements. Note that PPM signal sets can easily achieve values of $\rho \approx 1$ at these error-probability levels without the need for complicated encoding (Figure 3-4). It is evident from Figure 3-6 that the optical system achieves 30- to 40-dB higher transmission rates than the microwave system at any range Z, hence can deliver imaging data at the rate of 10^8 to 10^9 nats/s from Jupiter as compared to the roughly 10^5 nats/s capability of the Voyager-Goldstone link. It should be pointed out that both the optical and the microwave transmitters require similar prime power, since 10 to 100 W must be expended to drive the relatively inefficient lasers to the specified power levels, while the microwave transmitter aboard the Voyager spacecraft is generally operated at prime power levels of 50 to 100 W.

More reliable scientific data ($PSE \sim 5 \times 10^{-5}$) can also be transmitted via PPM-modulated optical beams at lower levels of ρ. In Section VII, a specific PPM-modulated signal set that is compatible with present-day pulsing techniques is shown to achieve information rates of $\rho = 0.32$ nats/photon at $PSE = 5 \times 10^{-5} \propto \exp(-10)$, while Reed-Solomon encoded PPM sets can achieve values of $\rho \gtrsim 1$ at similar error probabilities at the expense of added system complexity (Reference 3-1). It should be pointed out that even if the assumed average power levels of 1 W or more cannot be achieved, a significant improvement over present-day RF links might still be possible. For example, if the transmitter can only deliver 0.1 to 1 W of average optical power, the data-rate advantage of the optical system over the current high-performance RF link decreases to 20- to 30-dB. However, this is still a very significant improvement in terms of communication capabilities.

SECTION IV

ATMOSPHERIC EFFECTS

Weather conditions can be divided into three broad categories:
clear/turbulent, weak-scattering and strong-scattering. Clear weather
is characterized by negligible absorption, Rayleigh scattering and
weak to strong turbulence. Weak scattering conditions imply increased
absorption and mild Mie scattering in addition to turbulence. Cloudy
or overcast skies generally imply strong absorption, severe Mie
scattering, and significant delay dispersion effects. We shall
examine each of the above cases and evaluate their impact on receiver
design.

A.   CLEAR-WEATHER EFFECTS

Narrow transmitted beams arriving at the surface of the Earth
from interplanetary distances have generally expanded to effective
diameters on the order of 10 to 10,000 km. The receiver therefore
views what appears to be an infinite plane wave. Spatial and temporal
effects can therefore be described accurately in terms of the inter-
action of infinite plane waves with atmospheric inhomogenieties, and
such narrow-beam effects as beam steering and beam spreading can be
ignored. Clear-weather power absorption is strongly wavelength
dependent, corresponding to selective narrowband absorption by atmos-
pheric constituents (carbon dioxide, ozone, and water vapor); hence,
the carrier wavelength must be carefully chosen to avoid these absorp-
tion bands. Scattering due to atmospheric molecules (called Rayleigh
scattering) tends to be insignificant in the optical region of the
spectrum.

Atmospheric turbulence effects often dominate during clear-
weather conditions. Turbulence is due to random variations in the
index of refraction of the atmosphere and leads to image dancing, beam
steering, beam spreading, scintillation, and spatial coherence degrada-
tion. When the receiver observes infinite plane waves, the most
important effects of atmospheric turbulence on these waves are
image-dancing, scintillation, and spatial coherence degradation. All
of these effects can be minimized by opening up the receiver's field-of-
view (typically $10^{-12} \leq \Omega_r \leq 10^{-10}$ sr) to observe more spatial modes
(Reference 2-1). (More complicated techniques can be envisioned,
involving independent mode processing, image tracking, etc., but these
methods will not be considered here.)

Atmospheric inhomogenieties also give rise to multipath effects.
Different phase fronts arriving with slightly different time delays can
combine to cause random interference at the receiver. When the delay
difference between various paths becomes comparable to the signal
duration, severe fading and signal distortion can result. The expected
value of the time-delay dispersion, t_d, therefore limits the channel
bandwidth to $B_c \simeq 1/2t_d$ Hz. For clear-air turbulence, the value of t_d

is on the order of 10^{-10} to 10^{-9} s, hence delay dispersion does not seem to cause a problem in this application unless extremely wideband signals are employed (Reference 2-1). Photon-counting receivers designed to operate under clear-weather conditions are therefore characterized by wideband capabilities and narrow fields-of-view.

If an optical uplink is used for spatial synchronization, the uplink beam should be narrow to ensure reasonably high field intensity near the deep-space vehicle. Infinite plane-wave approximations cannot be made in this case, and turbulence-induced beam-steering and beam-spreading effects must be properly accounted for. The standard deviation of the planar beam-steering angle, δ_{H}, depends on the turbulence path length, but generally is on the order of 1 to 10 μrad for moderate turbulence (Reference 4-1). Increasing the uplink beamwidth to greater than δ_{θ} compensates for this effect, at the cost of diluting the uplink power at the spacecraft. Since prime power at the surface of the earth is relatively inexpensive, it should not be difficult to design the uplink beacon for worst-case turbulence conditions. Beam spreading tends to further dilute uplink power, but this effect is generally not very severe and can again be accounted for by increasing the uplink power.

B.   WEAK-SCATTERING CONDITIONS

Weak-scattering or low-visibility conditions are the result of scattering by aerosols in the atmosphere. These particles (smoke, dust, water droplets, etc.) are typically large compared to a wavelength and give rise to Mie scattering and power absorption effects, which must also be considered in addition to turbulence. The coherence function tends to become narrow in this case. Again, multimode operation is suggested, requiring still wider fields-of-view. The most advantageous processing scheme depends strongly on the degree of scattering, but typically both coherent (possibly turbulent) and scattered components have to be observed (References 2-1 and 2-2). Power absorption depends on the type and extent of scatterers, and may be in the neighborhood of 6 dB for moderate visibility conditions (Reference 4-1). The increased field-of-view required to collect scattered energy forces the receiver to observe more background modes as well, and therefore some degradation in system performance can be expected. Delay dispersion effects tend to increase, further limiting the channel bandwidth. In the uplink beam, scattering and absorption losses must be accounted for by further increases in beam power. High-rate communication still appears feasible under these conditions (perhaps at higher error probabilities), but more research is needed to obtain quantitative data on moderate- to low-visibility channel parameters and their impact on system design.

C.   STRONG SCATTERING CONDITIONS

In this category we include anything from light fog near the receiver to thick clouds completely obstructing the view. Absorption and scattering are very severe, again depending on local conditions. Laser propagation experiments through clouds indicate that even with a 5×10^{-3}-sr receiver field of view, 10- to 20-dB power losses are typical (Reference 1-1) and pulse delay dispersions on the order of 1 to 10 µs have been observed. These figures apply only to one set of experimental conditions, and might vary substantially for a different locale.

Severe scattering and absorption generally extinguish the coherent component altogether, and the normalized received field coherence function tends to approach a unit impulse. If spatial synchronization could somehow be maintained, multimode spatial and temporal processing techniques might be attempted to recover some of the scattered radiation and possibly achieve a reliable link at reduced rates (References 2-1 and 2-2). The uplink beacon approach does not appear feasible in this case due to severe absorption and scattering near the beacon. Other spatial synchronization techniques have to be explored if optical communication through strong-scattering channels is to become feasible.

D.   SOME ADVANTAGES OF TERRESTRIAL RECEIVERS

Despite the numerous problems introduced by the atmosphere, terrestrial optical receivers enjoy some definite advantages over possible Moon-based and orbiting counterparts. The most obvious advantage is availability for repairs, realignment and routine maintenance operations without the need for a costly space venture.

The feasibility of constructing very large terrestrial optical antennas with relative ease should not be overlooked. Segmented optical antennas with diameters exceeding 10 m can be constructed on existing microwave pedestals, and 10 to 100 µrad fields of view appear feasible (Reference 3-2). Pointing and tracking these antennas to the required accuracy can be achieved by improved microwave antenna technology. Furthermore, all of the optical components and techniques required for the construction of large aperture, Earth-based, photon-counting receivers are in existence at the present time (References 3-2 and 4-2).

The availability of virtually unlimited prime power (that is, 1 to 10 kW) for driving the uplink beacon assures accurate closed-loop tracking and pointing at both ends of the optical link when favorable weather conditions prevail.

E. SITE SELECTION

We can conclude that high-rate optical communication through clear or weakly scattering atmospheric channels appears feasible, even with relatively simple receiver structures. In contrast, high-rate optical communication through strong scattering channels with reasonable receiver structures appears to be very difficult at best, and probably impossible at the present time. It is therefore important to select receiver sites with great care, based on the probability of clear weather at any given time. If full-time coverage is required, then several receiver stations are needed around the globe to provide that coverage. Previous weather studies indicate that broad areas with less than 30 to 40% cloud cover each season exist in the Southwestern U.S., North Africa, Saudi Arabia, and Australia (Reference 4-3). The probability of reception can be increased by selecting several sites at each locale with uncorrelated (or only slightly correlated) weather patterns (Reference 4-4). For example, if n uncorrelated weather sites were located in the Southwestern U.S., and if each site was overcast with probability p, $(0 \leq p \leq 1)$, then the probability of clear weather over at least one of the n sites is P (clear) = $1 - p^n$. For the typical (although somewhat high) value of p $\simeq$ 0.3, it is obvious that three such sights (n = 3) would provide 97.3% probability of clear weather, while for n = 4 the probability of link availability increases to 99.19%. These might well be acceptable odds.

The possibility of using only a single locale (or perhaps two locales) for partial coverage should also be considered. With sufficient on-board data storage, the spacecraft could record data while the receivers are occulted by the rotation of the Earth. The recorded data could then be dumped at high rate when the receivers come into view. The amount of data-storage required depends on the data-rate and occultation time. The impact of large data-storage devices on spacecraft design should be investigated in greater detail.

Finally, the possibility of providing enough backup storage to record an entire mission should be investigated. With advances in magnetic-bubble, tape, and disc storage technology (References 4-5 and 4-6), an entire 10^{11}- to 10^{12}-bit mission might be recorded on board and dumped at high rate when favorable weather conditions prevailed. This approach would essentially eliminate the weather problem, and allow reliable high-rate data retrieval from the outermost reaches of the solar system.

SECTION V

SIGNAL SETS FOR DIRECT DETECTION RECEIVERS

Direct detection receivers respond only to variations in field intensity, hence signal sets compatible with direct-detection receivers must employ intensity modulated formats. Signal formats that employ narrow, low-duty-cycle pulses are particularly attractive from several viewpoints including ease of implementation, efficient use of available source energy, potentially high information capacity, and immunity to background interference. A pulsed signal format that encompasses all of the above characteristics and in addition achieves optimal performance under the MAP divergence criterion is M-ary PPM (Reference 2-1). A summary of its basic properties follows.

The M-ary PPM signal set can be described by referring to Figure 5-1. Each received symbol x_i in the set requires T seconds for transmission. The symbol interval is divided into M time slots of τ-seconds duration, hence $M = T/\tau$. Every symbol contains exactly one pulse, of mean photon count $K_S = n_S T$ in one of the τ-second time slots. The signal set can be ordered so that a pulse in the ith time slot corresponds to the symbol x_i; therefore, there are exactly M symbols, $M \geq 2$, ordered according to subscript. Each correctly decoded symbol carries exactly ln M nats of information. At the transmitter, the digital data is therefore partitioned into blocks of $(\log_2 e)$ (ln M) bits, and each such block transmitted as a unique M-ary PPM symbol. In the absence of interference, decoding errors occur only if no counts are observed in any slot during a synchronous T-second time interval. This occurs with probability exp $(-K_S)$ due to the Poisson distribution of counts. When symbol erasure occurs, the MAP decoder makes an equiprobable guess among the M symbols (assuming equiprobable symbol assignment) and guesses the correct symbol with probability 1/M. Hence the MAP symbol-error probability is

$$PSE = \left(\frac{M-1}{M}\right) \exp\ (-K_s) \tag{5-1}$$

while the equivalent bit-error probability becomes (Reference 2-1):

$$PE = \left(1/2\right) \exp\ (K_s) \tag{5-2}$$

Defining the photon information rate in nats/photon as

$$\rho = \frac{\ln M}{K_s} \tag{5-3}$$

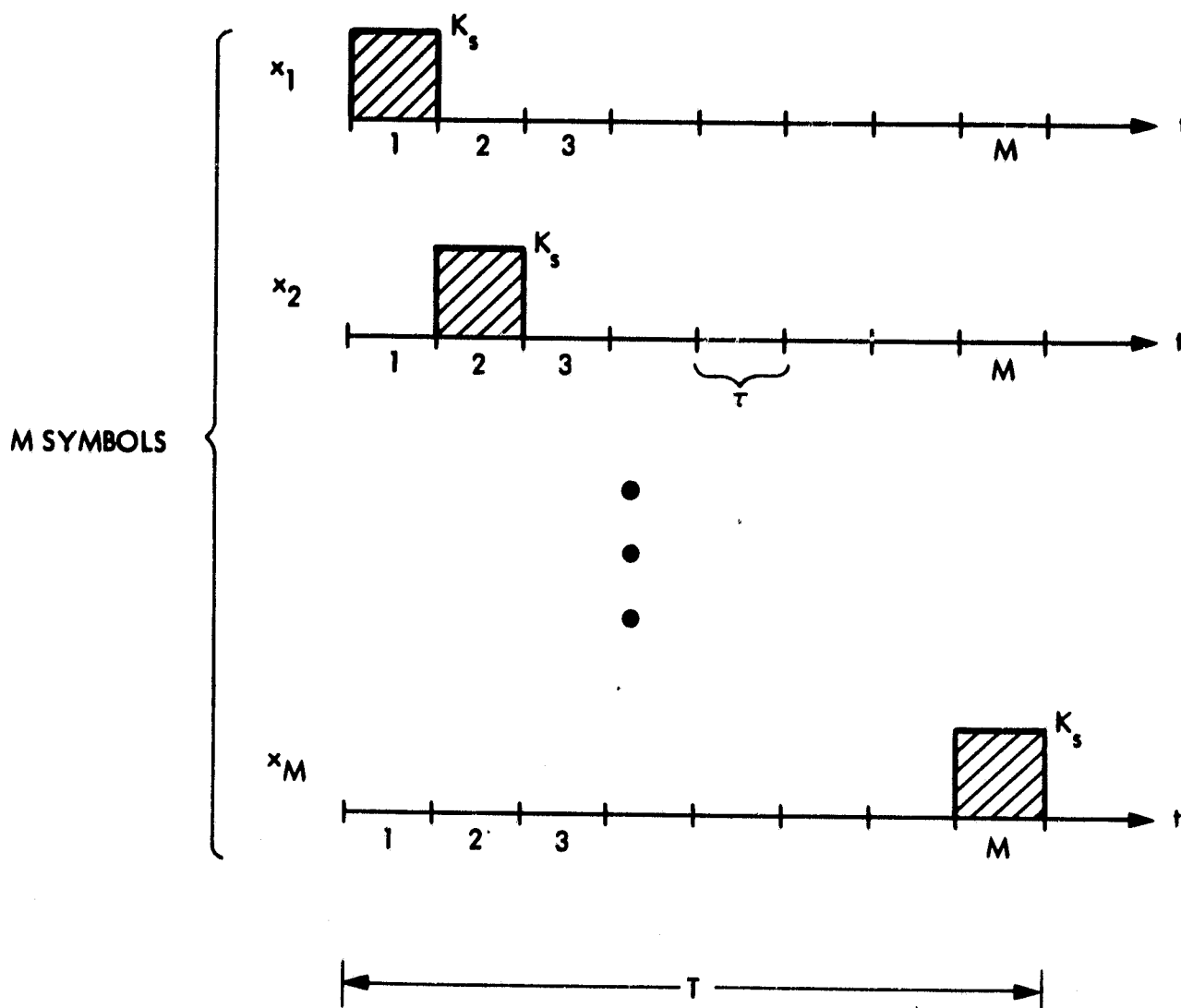the symbol error probability can be expressed as (References 2-1 and 3-1):

Figure 5-1.   M-ary PPM Signal Set

$$PSE = \left(\frac{M-1}{M}\right) M^{-1/\rho} \tag{5-4}$$

This function is represented in Figure 3-4. It can be seen that for $\rho > 1$, PSE decreases very slowly with increasing M, while for $\rho < 1$, PSE decreases rapidly with increasing M due to the relatively large value of the exponent $1/\rho$. This is the reason why information rates on the order of 1 nat/photon are easy to achieve at reasonable values of PSE, whereas high values of ρ lead to severe implementation problems with PPM signal sets.

The PPM signal set can theoretically operate at any desired transmission rate R, and at arbitrary values of ρ and ε, where

$$\varepsilon \triangleq \exp(-K_s) > PSE, \text{ for all } M \tag{5-5}$$

For example, let $R = R_o$, $\rho = \rho_o$ and $\varepsilon = \varepsilon_o$. Then, by simple substitution,

$$M = \varepsilon_o^{-\rho_o} \tag{5-6a}$$

$$T = \frac{\ln M}{R_o} \tag{5-6b}$$

$$K_s = \frac{\ln M}{\rho_o} \tag{5-6c}$$

The value of τ is determined from M and T, and the required average photoelectron count can be found from K_s and T.

M-ary PPM signal sets enjoy a large degree of immunity from external interference because all of the signal energy available in T seconds is concentrated in a τ-second interval, while the noise counts remain distributed over the entire T-second symbol duration. In Section VII it will be shown that external noise effects do not degrade MAP decoder performance until the average noise count rate becomes a significant fraction of the average signal count rate. That result enables us to determine conditions under which background (and dark-current) noise can be neglected, and suggest design procedures for achieving near-quantum limited performance even in the presence of external interference.

SECTION VI

POINTING AND TRACKING REQUIREMENTS

The inherent advantage of an optical communication link lies in its potential use of narrow optical beams for power concentration. This concentration leads directly to more information transmission for given source power over a given distance, or the extension of a fixed data rate to greater distances. However, narrow beams require accurate source pointing capabilities. Alternately, the ability to point the optical beam determines the ability to concentrate optical power and achieve the above advantages. Hence the spacecraft pointing operation is more intimately related to data transmission performance in optical systems than in RF systems. In this section, we examine this relationship.

The basic pointing operation can be described by the diagram shown in Figure 6-1. The receiving station moving with relative tangential velocity V_T transmits a beacon to the spacecraft at time T_1. The spacecraft makes use of the arriving beacon at time T_2, determines the lead-angle α, and points the downlink beam in the proper direction to intercept the ground receiver at time T_3. The spacecraft must, therefore,

(1) Acquire, measure, and track the received beacon line of sight.

(2) Compute and continually update the lead angle α.

(3) Point the optical beam in the desired direction.

Each of these operations has its own inherent error. The combined effect of all the errors produces the total pointing error (Figure 2) of the data return link. The minimal optical beam must encompass this pointing error to ensure reliable communications. Hence θ_t, the usable planar beamwidth of the data link, is limited to $\theta_t \gg 2\sigma_e$ rad, where σ_e is the standard deviation of the planar pointing error, θ_e. In the following sections, we examine the principle contributions to θ_e.

Optical pointing systems will generally have a form similar to that of Figure 6-3. After initial acquisition, the received beacon, which may be data-modulated, can be split for simultaneous data demodulation and beam tracking. The beam tracking generates an error signal that is used to keep the receiving optics aimed at the beacon. The tracking information in conjunction with spacecraft attitude sensing and transmitted location data is used to compute the point-ahead angle. The computed angle can be used to gimbal the transmitter antenna so as to properly point the optical data carrier. This system assumes the relative tangential velocity V_T is significant enough to require separate receive and transmit optics. Otherwise, common optics can be used, preserving boresight integrity and generally reducing the weight, cost, and complexity of the spacecraft.
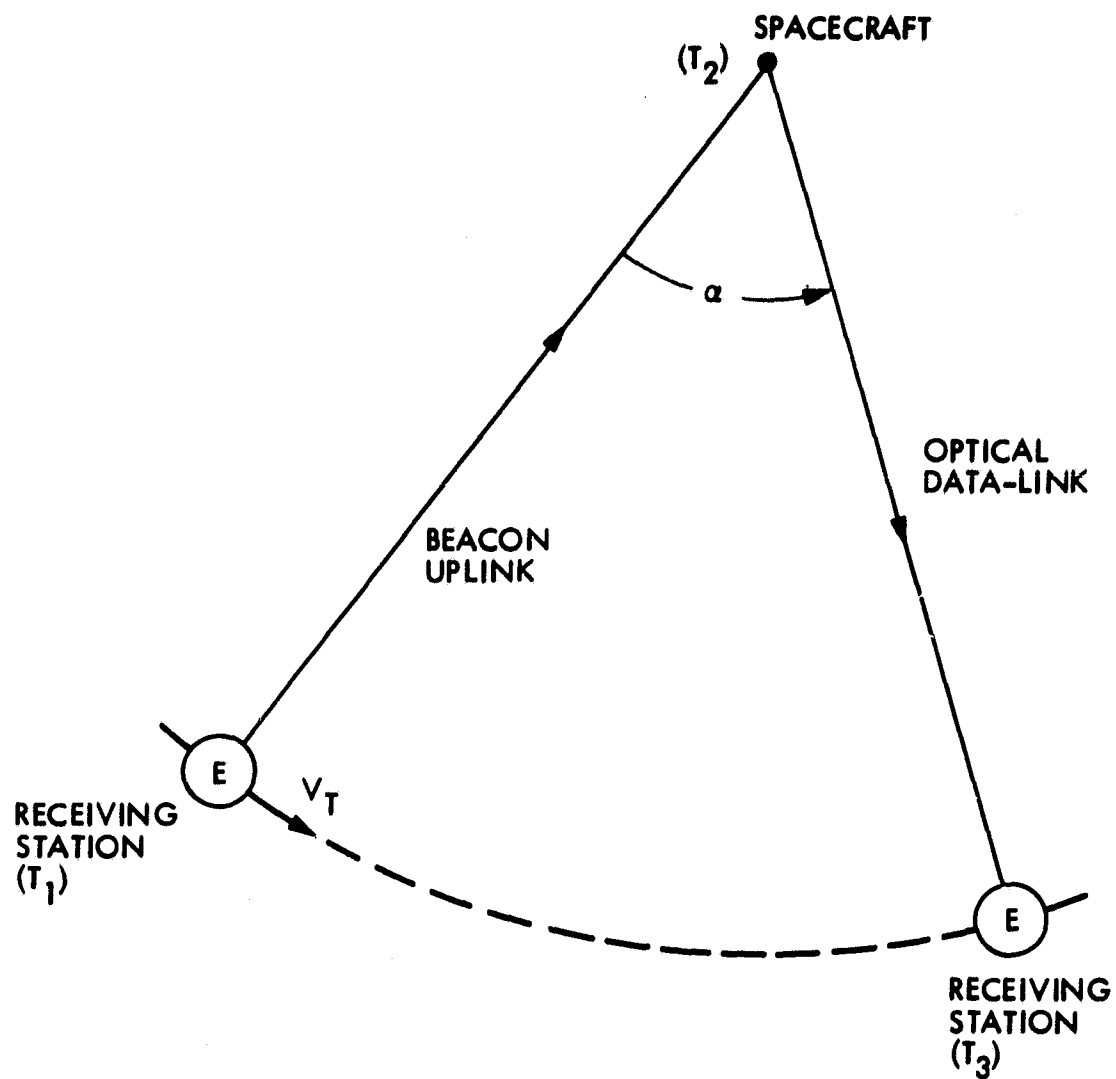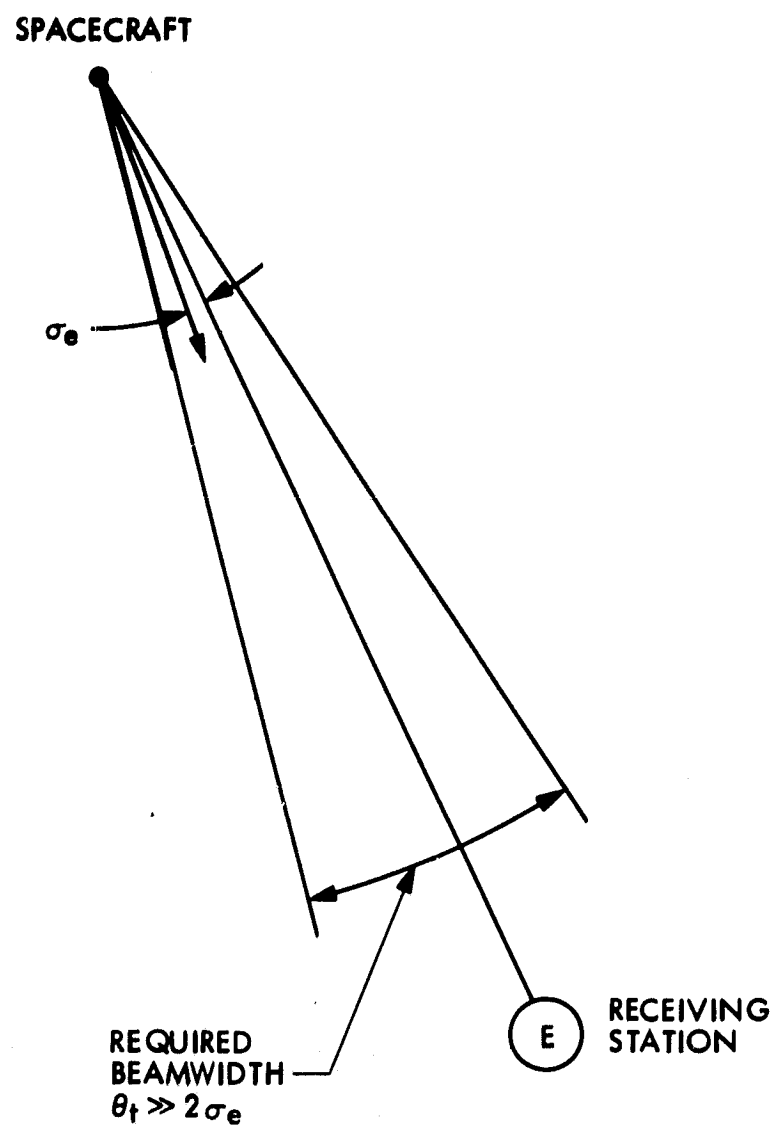
Figure 6-1. Point-Ahead Geometry

SPACECRAFT

σ_e

REQUIRED
BEAMWIDTH
$\theta_t \gg 2\sigma_e$

E RECEIVING
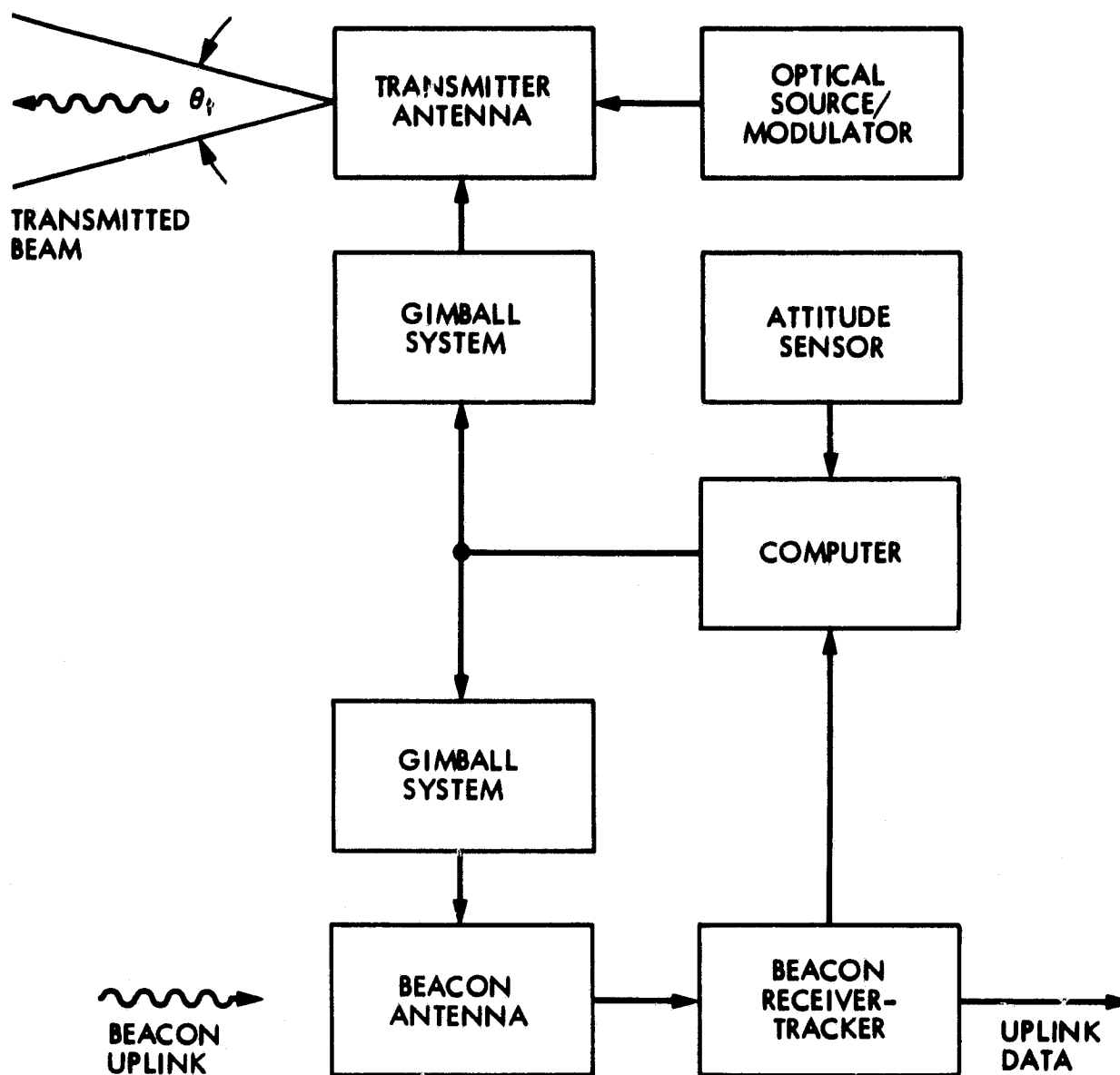STATION

Figure 6-2. Pointing Error and Beamwidth

Figure 6-3.   Optical Tracking and Pointing System

A. BEAM-TRACKING ERRORS

The spacecraft must try to determine the LOS (line-of-sight vector) of the arriving beacon field. Since the LOS may vary due to relative motion, it must be continually tracked by the spacecraft. The standard procedure for tracking the arriving beacon is to focus the field onto the crosshairs of a quadrant detector, and use azimuth and elevation error signals to control the gimballing of the receiver optics, keeping the LOS vector normal to the quadrant. If the LOS vector is normal to the quadrant, and if the relative velocity is known, then the required point-ahead is a fixed (computable) angle from the LOS. Hence, LOS tracking errors will convert directly to point-ahead errors even with precise point-ahead computation.

Considerations must also be given to bias errors caused by imbalance of the quadrant and by other optical sources entering the tracking receiver's field of view. Since the quadrant detector will track the center of gravity of all sources imaged on the detector, bright sources can steer the LOS pointing away from the desired beacon. The most serious hazards here are the possibilities of the Earth's illumination or a bright star entering the field of view, and introducing bias pointing errors many times greater than the rms error contributions of detector shot noise and thermal noise within the tracking circuits (References 6-1 and 6-2). More complicated tracking systems (using modulated beacons, for example) can also be used to reduce or eliminate the steering effects of background sources.

B. POINT-AHEAD COMPUTATIONAL ERRORS

The spacecraft must precompute the point-ahead angle for the return data link. The required angle α between the received beacon LOS and the return link is given approximately by

$$\alpha = \frac{2V_T}{c} \quad \text{radians} \tag{6-1}$$

where c is the speed of light and V_T is the relative tangential velocity between spacecraft and receiving station. The velocity V_T must be either communicated to the spacecraft or measured at the spacecraft. The former requires uplink data transmission by either modulating the beacon or by operating a low-rate auxiliary RF link, while the latter requires the spacecraft to have a separate ranging subsystem. If the velocity data is communicated to the spacecraft, the accuracy in α will depend on the accuracy with which the ground station can compute V_T, how often the computation is updated, and how accurately it is transmitted (quantized) to the spacecraft. If the spacecraft can recover V_T with a total error of ΔV_T m/s, then a pointing error of

$$\Delta u = \frac{2\Delta V_T}{(3 \times 10^8)} \quad \text{radians} \tag{6-2}$$

will result.

If the ranging operation is to be carried out at the spacecraft, it is necessary to superimpose ranging pulses on the optical data downlink and time synchronize the beacon transmitter to the ranging pulses at the ground receiver.

C.   DOWNLINK BEAM-POINTING ERRORS

After the LOS has been tracked and the point-ahead angle computed, the downlink optics must point the return data beam to the proper position. The accuracy with which the optics can be pointed in the desired direction depends on the following factors:

(1)   Attitude reference errors in the spacecraft. To point, the spacecraft must establish an attitude reference. This is generally accomplished by either a gyro-stabilized platform or via star and sun sensors. Gyro systems suffer from inherent drift effects that must be continually recalibrated. Star sensing requires tracking subsystems to align the spacecraft axis.

(2)   Mechanical and structural variations. Inherent vibrations, material stress, and component disturbances cause the axis of the spacecraft to become misaligned. These mechanical tolerances must be accounted for in error studies.

(3)   Boresight errors. The transmitting optics and gimbal mounts produce errors in aiming a narrow beam in the exact direction required. This problem is avoided if the received beacon and transmitted data use common optics, but must be considered when separate optical subsystems are used.

Although the contributions of the above error sources may be relatively small (usually less than 1 µrad) the primary difficulty is that these errors are open-loop errors that cannot be corrected unless the entire pointing operation is closed around the spacecraft receiver. This can be achieved by monitoring the received beam at the ground station and transmitting pointing corrections to the spacecraft. The magnitude of these error effects and the advantages of closing the entire pointing operation will have to be investigated further.

Experimental results carried out to date indicate that submicro-radian pointing accuracies can be achieved by closed-loop optical systems in a laboratory environment (References 6-2 and 6-3). Total dynamic errors due to structural vibration, gimbal control, torque motor noise, simulated relative motion, boresight alignment errors, and detector bias errors can be kept below 0.60 µrad rms. Furthermore, acquisition

operations were generally found to require no more than six seconds on the average. These preliminary experiments indicate that accurate pointing of microradian transmitter beams ($\theta_t \approx 1$ μrad) are well within the capabilities of present-day technology.

SECTION VII

TRANSMITTER AND RECEIVER STRUCTURES

In this section, some specific laser sources noted for high power and efficiency are considered, and a PPM modulation scheme conforming to laser constraints is examined. The structure of the MAP decoder for PPM signals is described, and receiver performance evaluated in the presence of external interference.

A. OPTICAL TRANSMITTER STRUCTURES

The most effective sources of intense, narrowband radiation at the present time are lasers. Lasers can be designed to operate anywhere from the UV (ultraviolet) to the FIR (far-infrared) regions of the spectrum, covering the wavelength range from 0.1 to 100 µm. With a few notable exceptions, most lasers are extremely inefficient, with typical efficiencies ranging from 0.1 to 1 percent. These lasers therefore require 100 to 1000 W of prime power for every watt of usable optical output. Present spacecraft power allocation for communications is typically less than 100 W, which makes it difficult to achieve average optical power levels of 1 W or more. The exceptions are the CO_2 and CO gas lasers with efficiencies exceeding 10 percent, and the semiconductor lasers (and coherent arrays) that can reach efficiencies of 10 to 20 percent or more. The gas lasers are relatively complicated, and operate at wavelengths of 10 and 5 µm respectively, where high-gain detectors are not presently available and where beam diffraction effects are severe. In contrast, semiconductor lasers (and coherent laser arrays) are small, lightweight devices that operate near $\lambda = 1$ µm where high-gain, high-quantum efficiency detectors are available and beam diffraction effects are potentially less objectionable. In the future, maximum power levels of 20 to 30 W and average power levels of 1 W or more may be possible with coherent arrays, requiring only 5 to 10 W average input power. These semiconductor laser arrays therefore appear to be uniquely qualified for deep-space application, offering high power and efficiency together with reliable construction and light weight. The following discussion will therefore be geared towards transmitters employing semiconductor laser arrays, although the concepts discussed apply to other laser sources as well.

A more detailed diagram of the optical transmitter is shown in Figure 7-1. The digital data stream is block-encoded into intensity-modulated channel symbols, notably M-ary PPM. The modulator-driver subsystem pulses the laser at the appropriate time to generate one of the M-channel symbols. Several methods are available for pulsing lasers, including intracavity Q-switching, mode-locking, and current-pulsing (Reference 7-1). Semiconductor lasers are normally current-pulsed, generating optical pulses of roughly the same duration as the pulsed current. Pulse-widths ranging from less than one nanosecond to several microseconds can be generated in this way.
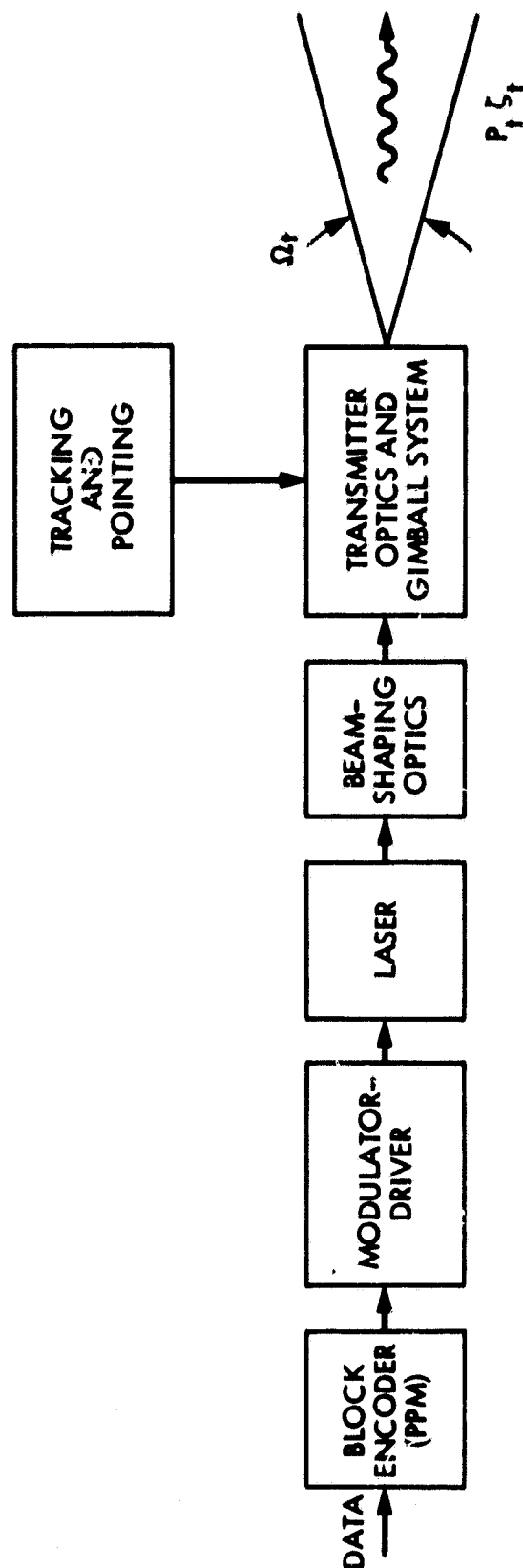
Figure 7-1. Optical Transmitter Structure

Consider the design of a PPM signal set operating with 4 percent duty-cycle constraint.[2] If the background radiation is not too severe, symbol error probability is governed by Equation (5-1) and ε is defined by Equation (5-5). Letting $\varepsilon = \exp[-10]$ implies that $K_s = 10$; therefore, on the average, 10 photoelectrons have to be generated at the receiver for each symbol to achieve the specified value of ε. Due to the duty-cycle constraint, we must have $\tau/T = 4 \times 10^{-2}$, or $M = 25$. The information rate is therefore $\rho = 0.32$ nats/photon. If we allow higher error probabilities, such that $\varepsilon = 10^{-2}$, for example, then we can achieve $\rho = 0.7$ nats/photon with this scheme. We have therefore demonstrated a simple modulation format that achieves high information rates, with 1-W average transmitted power.

The modulated optical beam passes through beam-shaping optics that spatially match it into the transmitting antenna, which in turn expands, collimates, and transmits the beam in the proper direction. Since the average transmitted power is assumed to be 1 W, Figure 3-2 can be used to determine the normalized photoelectron rate $n_s/A_r \zeta_r \eta$. Assuming that the receiver is a large photon bucket, the performance curves of Figure 3-6 are obtained. (Note that the transmission rate decreases with distance since τ must be increased to maintain an average of 10 photons/symbol, however the duty cycle must remain unchanged.)

While efficient, high-power lasers have obvious advantages for deep-space communications, the potential use of less efficient lasers (such as Nd:YAG, 0.1 percent efficient) should not be overlooked. Sun-pumped Nd:YAG lasers have recently been developed with excellent beam quality, reasonable power levels, and potentially long life (Reference 6-3). Although available solar energy decreases rapidly with distance, the possible use of large-aperture optics for solar-energy utilization in deep-space applications deserves further consideration.

B.   OPTICAL RECEIVER STRUCTURE

The structure of the optical MAP receiver is shown in Figure 7-2. After acquiring the transmitter, the receiver antenna tracks the incoming optical field to keep it within its field of view. This operation can be accomplished by a tracking subsystem of the type described in Section VI, where now the received field acts as the beacon.

If the atmosphere is clear and calm, the received field is essentially coherent over the entire aperture and the spatial filter can be adjusted to observe only one, or perhaps a few, spatial modes. Under weak scattering or highly turbulent conditions, the spatial filter can be readjusted to observe more spatial modes, while filtering out those

---

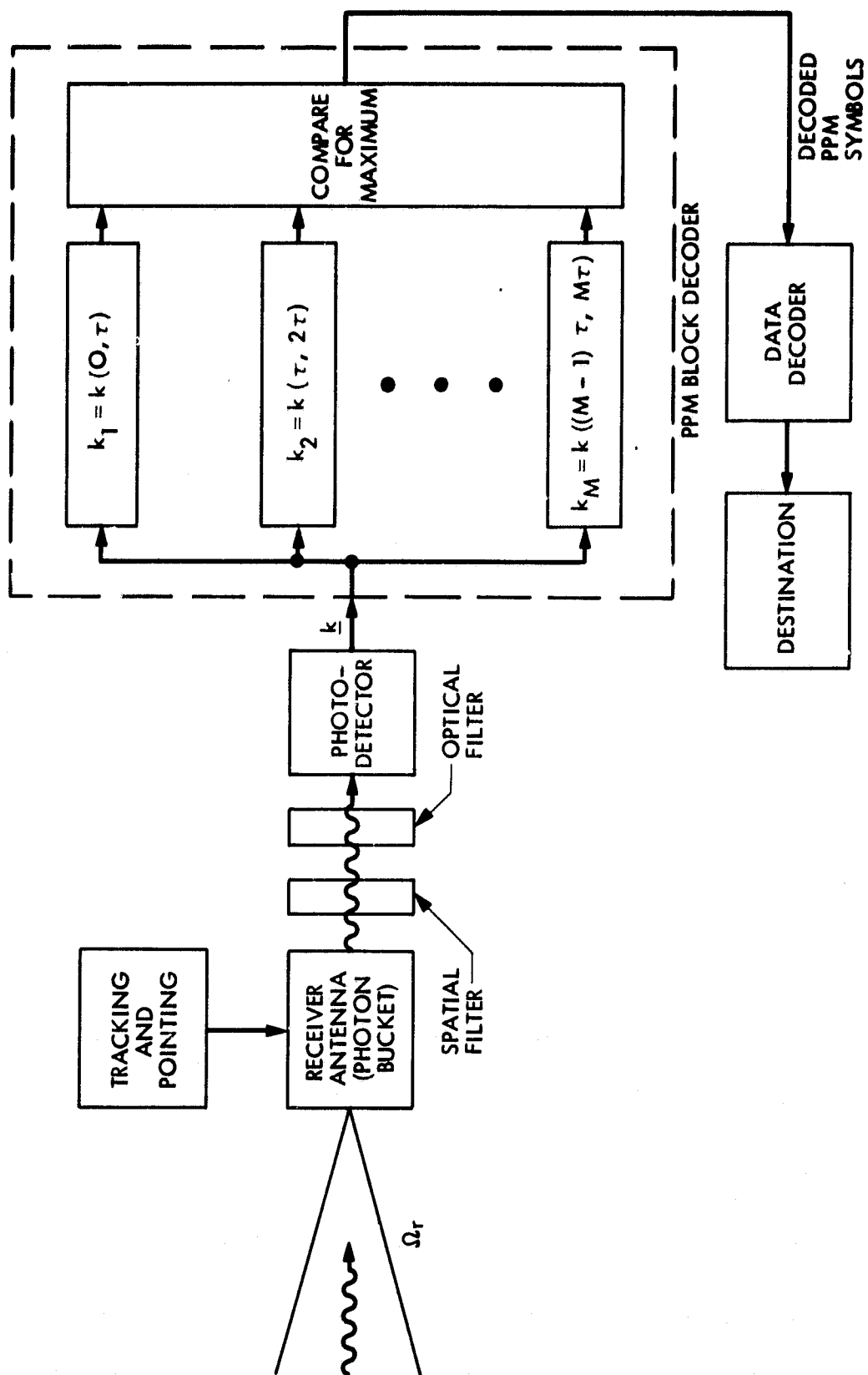[2]This duty factor is reasonable for cryogenically-cooled semiconductor lasers.

Figure 7-2. Optical MAP Receiver Structure

modes that contain little signal power, and are excited primarily by background fields. The spatially filtered fields are passed through a narrow-band optical filter to further reduce background interference.[3] The spatially and temporally filtered fields are focussed onto the active surface of a cooled, high-gain photomultiplier tube that generates photoelectrons in response to the impinging signal and background fields. Dark current electrons also contribute to the detector output. The output current can be represented by a discrete count vector $\underline{k} = (k_1, k_2, \cdots, k_M)$ over each synchronous T-second time interval. The M components represent counts over each τ-second subinterval. If the inverse of the optical predetection filter bandwidth is much less than τ (which is almost always the case) then the count components k_i can be modeled as Poisson-distributed random variables with mean value $K_s + K_n$ when both signal and background fields are observed, and K_n when only background fields and dark current counts are present (recall that $K_s = n_s T$ whereas $K_n = (n_b + n_d)\tau$). Under these conditions, the structure of the MAP receiver is well known (Reference 2-1). For equiprobable symbols, the decoder stores each component of the vector $\underline{k}$, and selects that symbol that corresponds to the highest count. Errors occur if $k_i \geq k_q$, $i \neq q$, when in fact x_q was transmitted. In case of a tie, the MAP decoder makes an equiprobable guess. The probability of symbol error is given by the expression (Reference 2-1):

$$PSE = 1 - \left\{ \frac{\exp\left[-(K_s + MK_n)\right]}{M} \right\}$$

$$- \sum_{r=0}^{M-1} \sum_{k=1}^{\infty} \text{Pos}\,(k,\, K_s + K_n) \left[\sum_{j=0}^{k-1} \text{Pos}\,(j,\, K_n) \right]^{M-1-r}$$

$$\times \left[\text{Pos}\,(k,\, K_n)\right]^r \frac{(M-1)!}{j!\,(M-1-r)!\,r+1} \tag{7-1}$$

where $\text{Pos}\,(x,\, y) = \dfrac{y^x}{x!}\, e^{-y}$.

---

[3]Filters with 10 to 100 Å bandwidths are readily available. State-of-the-art filters with bandwidths less than 1 Å can also be constructed at the cost of reduced optical transmission in the filter passband.

This function has been computed for various values of K_s as a function of M and K_n. Figures 7-3 and 7-4 show the results for $K_s = 20$ and $K_s = 40$. When $K_n = 0$, the symbol error probability becomes $PSE = (1 - 1/M) \exp(-K_s)$ where the coefficient is due to the fact that in case of an erasure, the MAP decoder makes a random choice among M equilikely possibilities and inadvertently chooses the correct symbol with probability $1/M$. As the noise level increases, errors due to noise also begin to occur, in addition to erasures.

Additional insight into the behavior of PPM signals in the presence of noise can be obtained from Figure 7-5, which shows PSE as a function of symbol energy K_s in the presence of various ratios of external noise to signal rates. Note that no significant performance deterioration takes place until the average noise count rate exceeds (roughly) one percent of the average signal count rate, that is $n_n/n_s > 10^{-2}$. For lower values of external noise, errors due to erasures dominate. It is therefore a relatively simple matter to determine when background effects must be taken into consideration, and when these effects can be safely ignored. In Appendix B we examine background levels under typical operating conditions and conclude that background fields can nearly always be ignored by photon-counting MAP receivers, if the receiver field of view is sufficiently small.
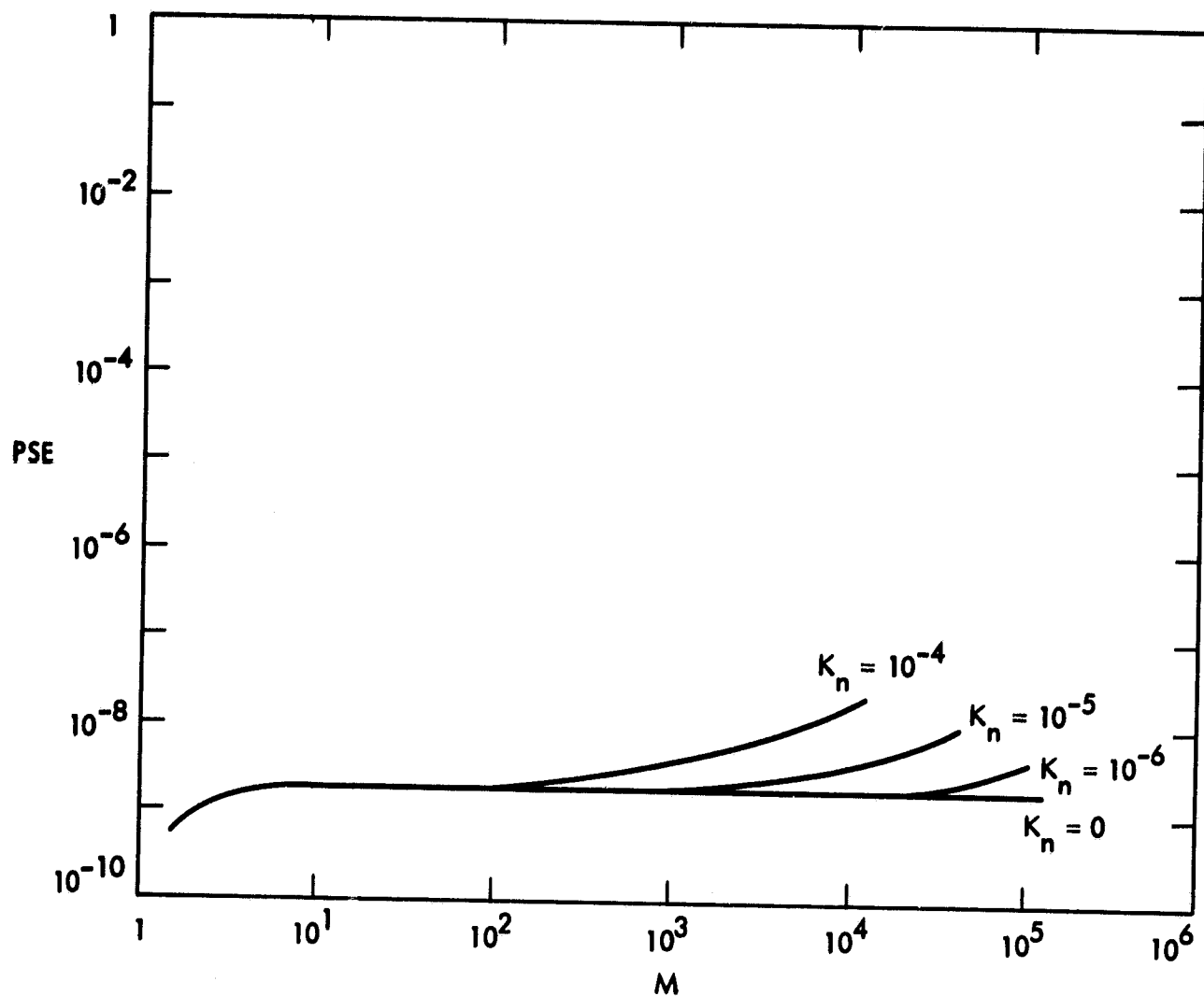
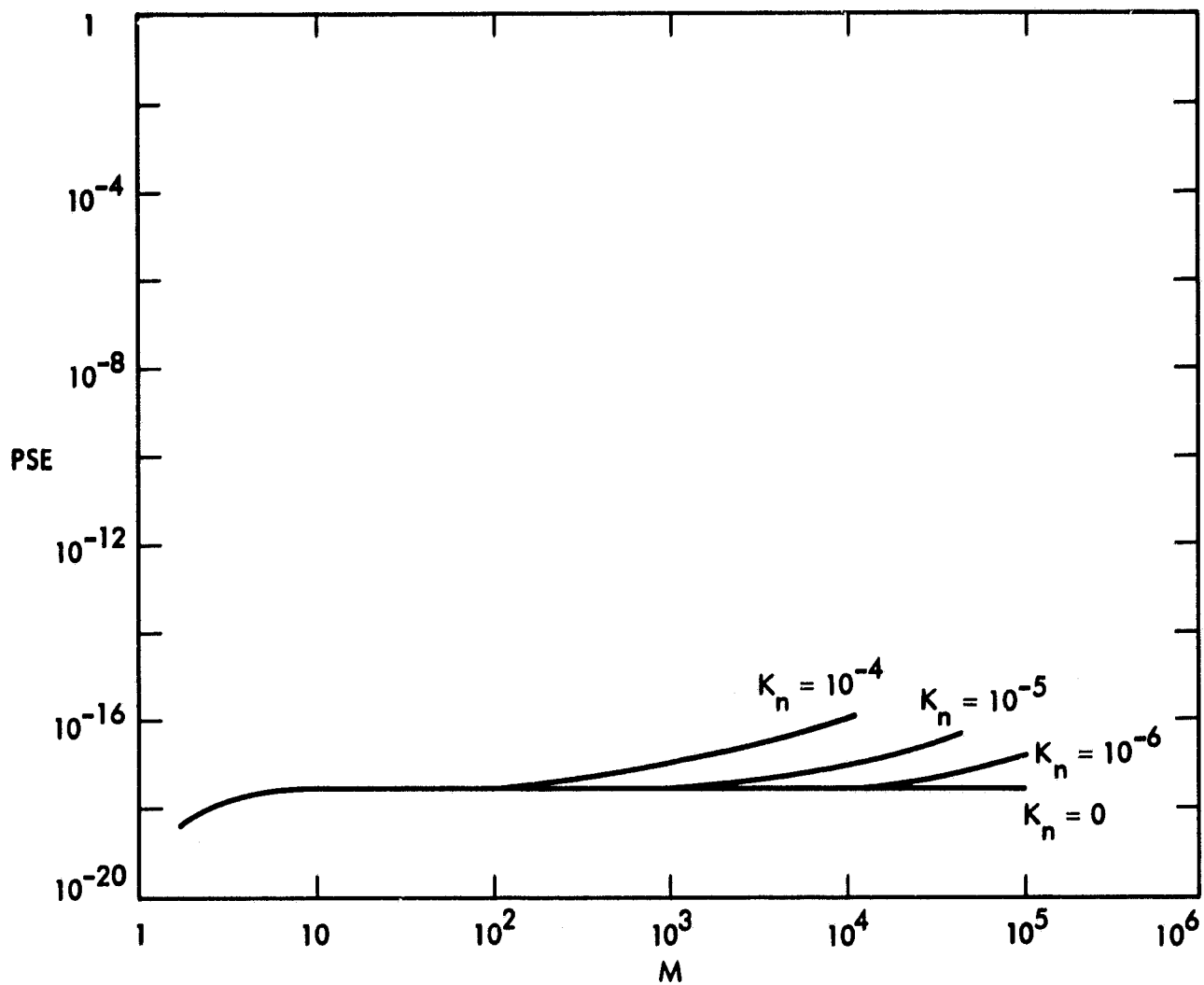Figure 7-3. PPM Symbol Error Probability as a Function of M and K_n, $K_s = 20$

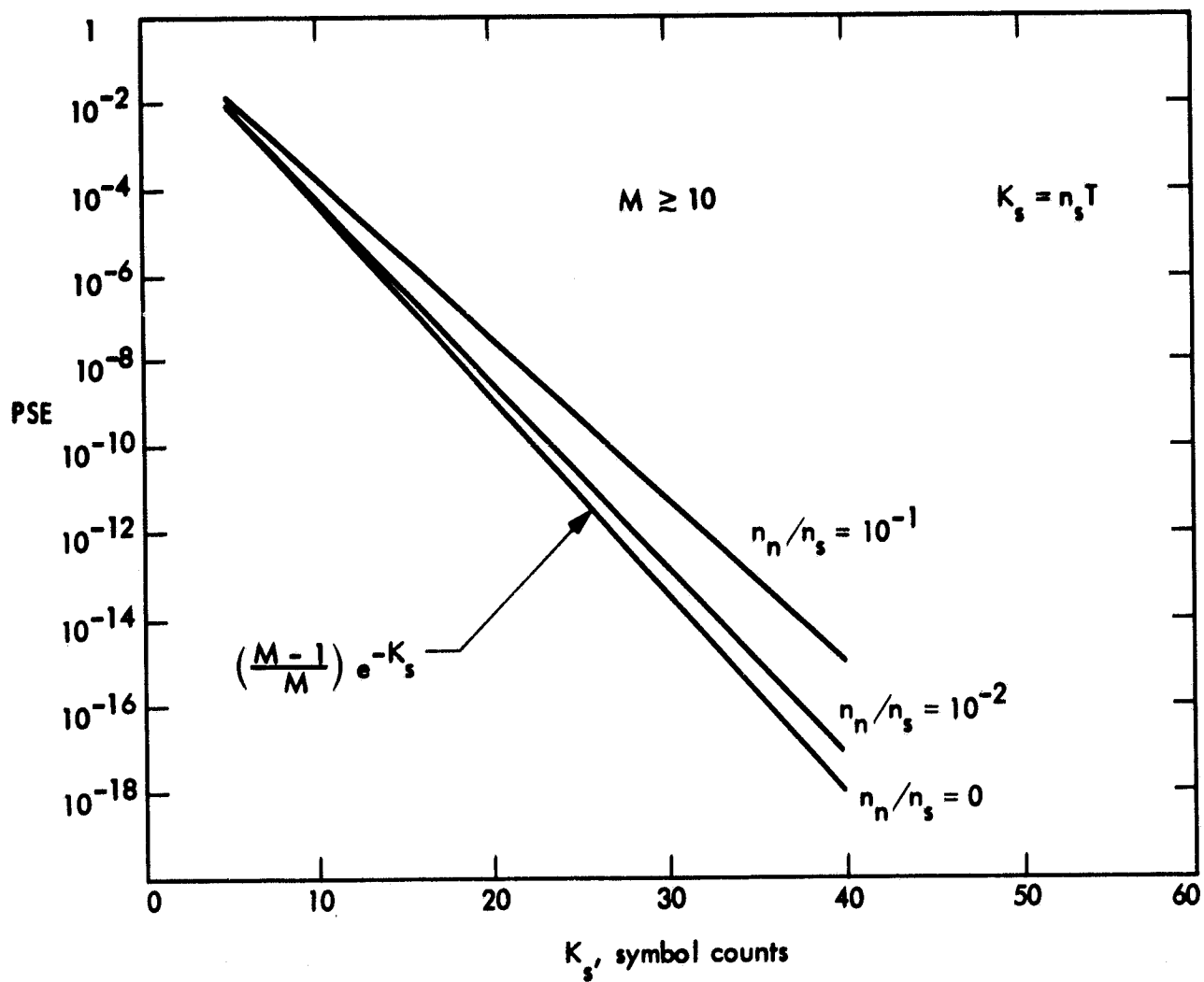Figure 7-4. PPM Symbol Error Probability as a Function of M and K_n, $K_s = 40$

Figure 7-5. PSE vs K_s for Various Ratios of n_n/n_s

SECTION VIII

CONCLUSIONS AND RECOMMENDATIONS

The potential advantages of optical communication systems for deep-space applications have been clearly demonstrated in this report. The main advantages over existing high-performance RF systems are the possibility of 30- to 40-dB increase in transmission rate at any range, or 15- to 20-dB range extension at comparable data rates. While terrestrial receivers suffer from atmospheric effects such as turbulence, unfavorable weather and scattered light (in addition to daily occultation of the spacecraft by the rotation of the Earth), orbiting or Moon-based receivers could essentially escape all of the above problems and routinely achieve the improvements predicted by the foregoing analysis. The performance improvements are the direct result of increased antenna gain at optical frequencies, necessitating extremely accurate pointing and tracking operations at both ends of the link. The main components of the spatial synchronization problem have been outlined, although more extensive analyses are needed to assess system pointing and tracking capabilities, and determine accurate bounds on usable transmitter antenna gain. In addition, studies should be initiated to determine if the capabilities of existing (efficient) optical sources are consistent with antenna gain and source-power requirements, and to indicate directions for future research if necessary.

Modulation formats deserve further attention. In particular, high-information-rate signal formats compatible with known modulation techniques need to be developed and evaluated, and their impact on receiver complexity determined. Future studies should include deep-space links employing extraterrestrial receivers, due to the advantages inherent in avoiding the terrestrial atmosphere. Since the optical free-space channel can often be modelled as an erasure channel, receiver structures and encoding schemes designed specifically to take advantage of the properties of this erasure channel should be investigated.

Finally, experiments are needed to complement the analytical studies, and to obtain system parameters not readily available by other means. Mechanical and structural variations, gyro-system stability, and boresight errors could all be investigated in the laboratory. Initial simulation experiments can easily be performed on the ground to prove concepts and evaluate component capabilities. More advanced beacon-tracking, beam-pointing, and decoding experiments could eventually be performed aboard the Space Shuttle, or on future deep-space missions using small, lightweight optical communications packages designed exclusively for system performance evaluation rather than actual data transmission. Terrestrial receiving stations are ideally suited for this purpose, since evaluation experiments could be initiated on command and carried out under the most favorable weather conditions, thus eliminating dependence on the weather. Simple, relatively inexpensive terrestrial receiving stations can be readily constructed

with a minimum expenditure of time and effort. Small, "scaled-down" versions of optical transmitters could be employed in such experiments with minimal impact on spacecraft design. The results could then be extrapolated reliably to evaluate design parameters and predict the performance of future deep-space optical communications systems.

REFERENCES

1-1. *Proceedings of the IEEE*, Special Issue on Optical Communications, Vol. 58, No. 10, pp. 1407-1786, October 1970.

1-2. J. R. Pierce, "Optical Channels: Practical Limits with Photon-Counting," *IEEE Trans. on Communications*, Vol. COM-26, No. 12, pp. 1819-1821, December 1978.

2-1. R. Gagliardi and S. Karp, *Optical Communications*, J. Wiley, New York, New York, 1976.

2-2. V. A. Vilnrotter, *Focal-Plane Processing for Scattered Optical Fields*, Ph.D. Thesis, University of Southern California, Los Angeles, 1978.

3-1. R. McEliece, L. Welch, "Coding for Optical Channels with Photon Counting," *DSN Progress Report*, Vol. 42-52, pp. 61-65, Jet Propulsion Laboratory, Pasadena, Calif., 1979.

3-2. R. F. Lucy, "Large Aperture Segmented Optics for Space-to-Ground Communications," *Applied Optics*, Vol. 7, No. 8, pp. 1571-1576, August 1968.

3-3. R. E. Edelson, B. D. Madsen, E. K. Davis, G. W. Garrison, "Voyager Telecommunications: The Broadcast from Jupiter," *Science*, Vol. 204, No. 4396, pp. 913-921, June 1, 1979.

4-1. W. K. Pratt, *Laser Communication Systems*, J. Wiley, New York, New York, 1969.

4-2. J. E. Jackson, L. B. Allen, T. E. Borham, "Paraboloidal Array of Spherical Segments for a Direct Detection Optical Receiver," *Applied Optics*, Vol. 9, No. 12, pp. 2798-2799, December 1970.

4-3. P. D. Potter, M. S. Shumate, C. T. Stelzried, W. H. Wells, *A Study of Weather-Dependent Data Links for Deep-Space Applications*, Technical Report 32-1392. Jet Propulsion Laboratory, Pasadena, Calif., October 15, 1969.

4-4. F. Kalil, *Optical and Microwave Communications - A Comparison*, TN D-3984, National Aeronautics and Space Administration, Washington, D.C., May 1968.

4-5. J. Egil Juliessen, "Where Bubble Memory will Find a Niche," *Mini-Micro Systems*, pp. 48-61, July 1979.

4-6. EDN Staff Report "Memory Devices," *Electrical Design News*, pp. 91-98, May 5, 1979.

6-1. M. A. Sheikh, <u>Statistical Analysis of Optical Beam Tracking Using Quadrant Detectors</u>, Ph.D. Thesis, University of Southern California, Los Angeles, 1977.

6-2. J. D. Wolf, "Precision Pointing and Tracking System for Space Laser Communications," SPIE Vol. 150, <u>Laser and Fiber Optics Communications</u>, pp. 9-14, 1978.

6-3. M. Ron, P. Freedman, J. Abernathy, G. Matossov, J. Wolf, J. D. Barry, "Space Optical Communications with the Nd:YAG Laser," <u>Proc. of the IEEE</u>, Vol. 66, No. 3, pp. 319-344, March 1978.

7-1. A. Yariv, "Quantum Electronics," J. Wiley, New York, New York, 1975.

A-1. Payne-Gaposchkin, C., <u>Introduction to Astronomy</u>, Prentice-Hall, Englewood Cliffs, N. J., 1958.

APPENDIX A

THE EFFECTS OF CIRCUIT NOISE AND DARK CURRENT ON RECEIVER DESIGN

In the foregoing analysis we have neglected the effects of circuit noise on receiver performance. In particular, we have not considered the effects of thermal noise generated by the load resistor (R) at the photodetector output. The thermal noise voltage generated by the load resistor can be modeled as a Gaussian white process with spectral level $N_{oc} = 4K \mathcal{F} R$, where K is Boltzmann's constant and $\mathcal{F}$ is the resistor temperature in degrees Kelvin. This noise process adds directly to the voltage generated by the detector current. Without internal detector gain, the rms thermal noise voltage is typically much greater than the voltage developed by a single electron flowing through the resistor. With sufficient internal gain, however, the effects of thermal noise can be overcome. It has been shown (Reference 2-1) that thermal environments can be overcome by ideal (that is, deterministic gain) photomultipliers if the gain satisfies the inequality $G \gg (2 \times 10^7)(\tau \mathcal{F}/R)^{1/2}$ where τ is the effective integration time. This can be seen in Figure A-1a, which is a graph of bit-error probability PE as a function of gain for binary PPM, with average signal and noise counts (K_s, K_n), pulse interval $\tau = 10^{-9}$ s, and load resistor $R = 50\Omega$, assuming room-temperature operation. Note that with gain $G \gtrsim 10^4$, PE becomes independent of G, implying quantum-limited performance. Similar results hold for higher dimensional signal sets as well.

Nonideal photomultipliers cannot achieve deterministic gain factors, but rather generate random gain that can be modeled as a Gaussian random variable with "spreading factor" ξ, which is usually taken to be a percentage of the mean gain. The effects of random gain on binary PPM error probability have been computed (Reference 2-1), and the results plotted in Figure A-1b for various values of mean gain G. It is evident that values of $\xi < 0.4$ do not affect PE for the range of mean gains considered. Hence quantum-limited operation can be achieved even with nonideal photomultipliers if sufficient gain is available and the spreading factor is not too great. Again, these results can be extended to higher dimensional signal spaces, and other values of K_s and K_n.

Finally, let us consider the effects of dark current. We have seen that dark current gives rise to random electrons (or groups of electrons, if $G > 1$) in the detector output process. These random electrons do not convey information to the decoder, and in fact serve to hinder the decoding operation. The generation of dark current electrons depends on the temperature of the emitting surface, its area, the type of photoemissive material used, and the particular design of the photomultiplier. The dark current rate, n_d, can be minimized by cooling the detector, reducing the emissive surface, and by careful design. Depending on type, dark current rates (measured at the photo-emissive surface) can generally be kept to values near $10 < n_d < 10^2$ by cooling and optimum design (Reference 4-1). Low-rate interference of this type has little impact on receiver performance, when M-ary PPM signal sets with short pulse durations are used. Detector dark current, therefore, does not interfere with quantum-limited operation in well-designed receivers, hence its effects can generally be ignored.
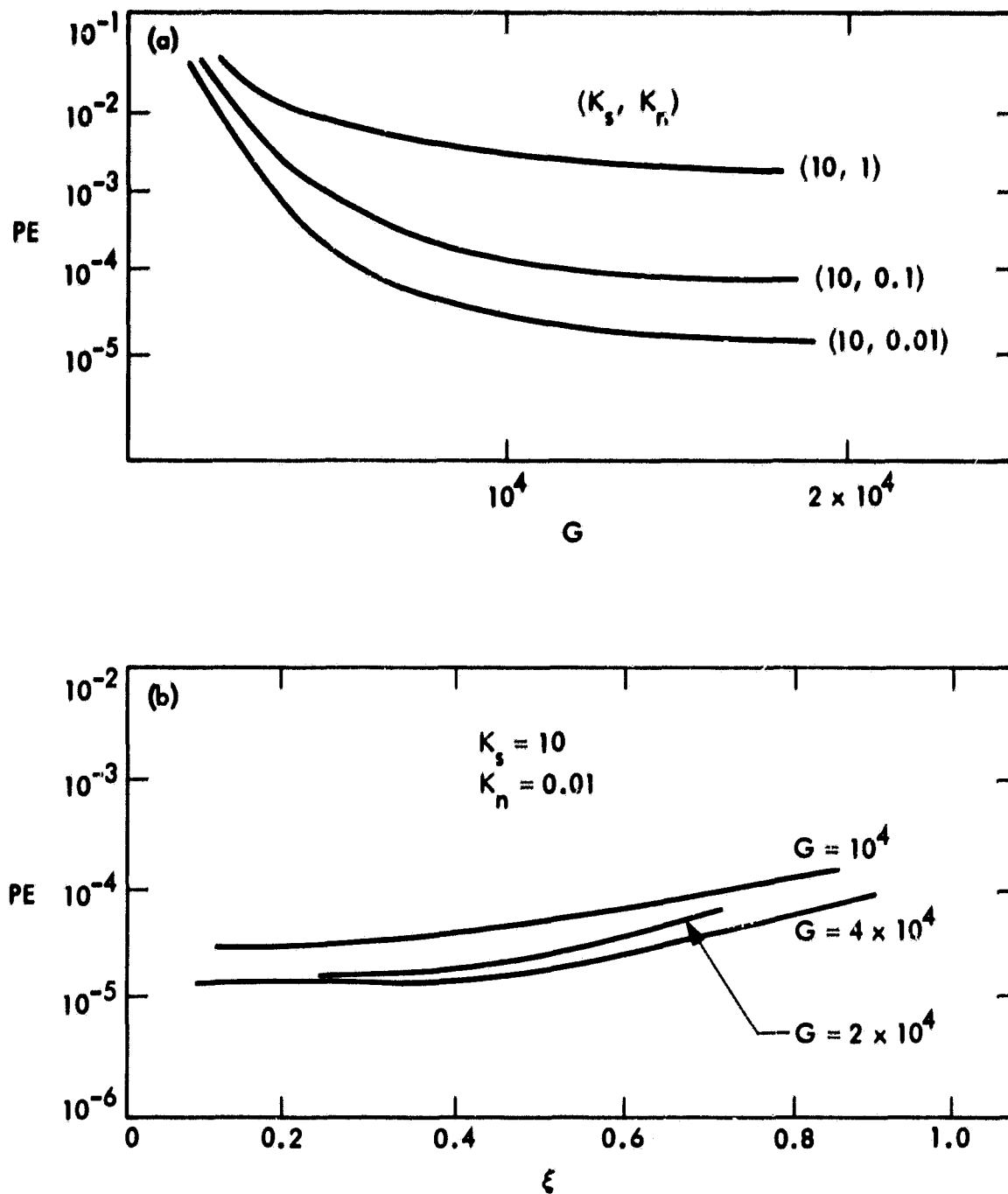
Figure A-1. PPM Error Probabilities in the Presence of Thermal Noise: (a) Error Probability vs Mean Gain G; (b) Error Probability vs ξ.

APPENDIX B

THE EFFECTS OF BACKGROUND NOISE ON SYSTEM PERFORMANCE

Background fields introduce random photoelectron counts into the detector output. The rate of these background-induced photoelectrons depends on the spectral irradiance of the interferring source, the bandwidth of the optical filter, center wavelength, receiver field of view, and the effective area of the collecting optics. Figure B-1 shows the normalized photoelectron rate due to various background sources as a function of receiver field of view (FOV) at $\Delta\lambda = 10$ Å.[4] (For other filter bandwidths, these results scale linearly.) Background noise counts increase with FOV for extended sources, but do not depend on FOV for point-sources such as stars. Note that "weak stars" (of visual magnitude +6 or more) contribute roughly 10^5 counts per second (or less) for each square meter of effective receiver area independent of FOV at $\lambda = 1$ μm. The number of stars of magnitude +6 or less is relatively small, however, and their locations are well known. Theoretically, communication can be avoided if the spacecraft passes in front of an interfering star, although the probability of such an encounter with narrow field-of-view receivers is practically zero. Planets are potentially more troublesome, since deep-space missions generally encounter planets by design. With receiver FOV of 10 μrad or less, the probability of the planet being seen by the receiver is still very small, and occurs only if the spacecraft passes directly in front of the planet. Noise contributions can be reduced by decreasing the FOV or the optical passband when possible. However, for terrestrial receivers, FOV must generally be kept greater than 10 μrad due to turbulence and scattering, which limit the utility of this approach. With 10 μrad FOV and $\lambda = 1$ μ, the receiver collects roughly 10^6 counts/m^2 from Jupiter. Since even a 1-W average power laser can delivery roughly 10-dB more counts from these distances (Figure B-2), the worst-case effect is a slight increase in error probability that can be countered by a 20 to 50 percent increase in average source power. (The performance degradation can also be alleviated by increasing the dimension of the signal space, since background noise effects become insignificant even for $n_b \simeq n_s$ when $M \geq 100$.) One of the main advantages of an orbiting receiver (besides the independence from weather) is the ability to reduce the FOV to values near 1 μrad or less. With such small fields of view, an orbiting optical receiver collects 20-dB fewer noise counts than its terrestrial counterpart (Figure B-3). Under those conditions, background noise effects can be completely ignored.

The possibility of having to receive optical transmission during the daytime is a potentially serious problem. It can be seen from Figure A-1 that even with excellent visibility, the background counts due to scattered sunlight tend to become severe, leading to degraded receiver performance. This problem is further aggravated as visibility

---

[4] These curves were compiled using published values of sky radiance and planetary and stellar spectral irradiance functions (Reference 4-1), together with the apparent dimensions of Jupiter viewed from the Earth during opposition (Reference A-1).
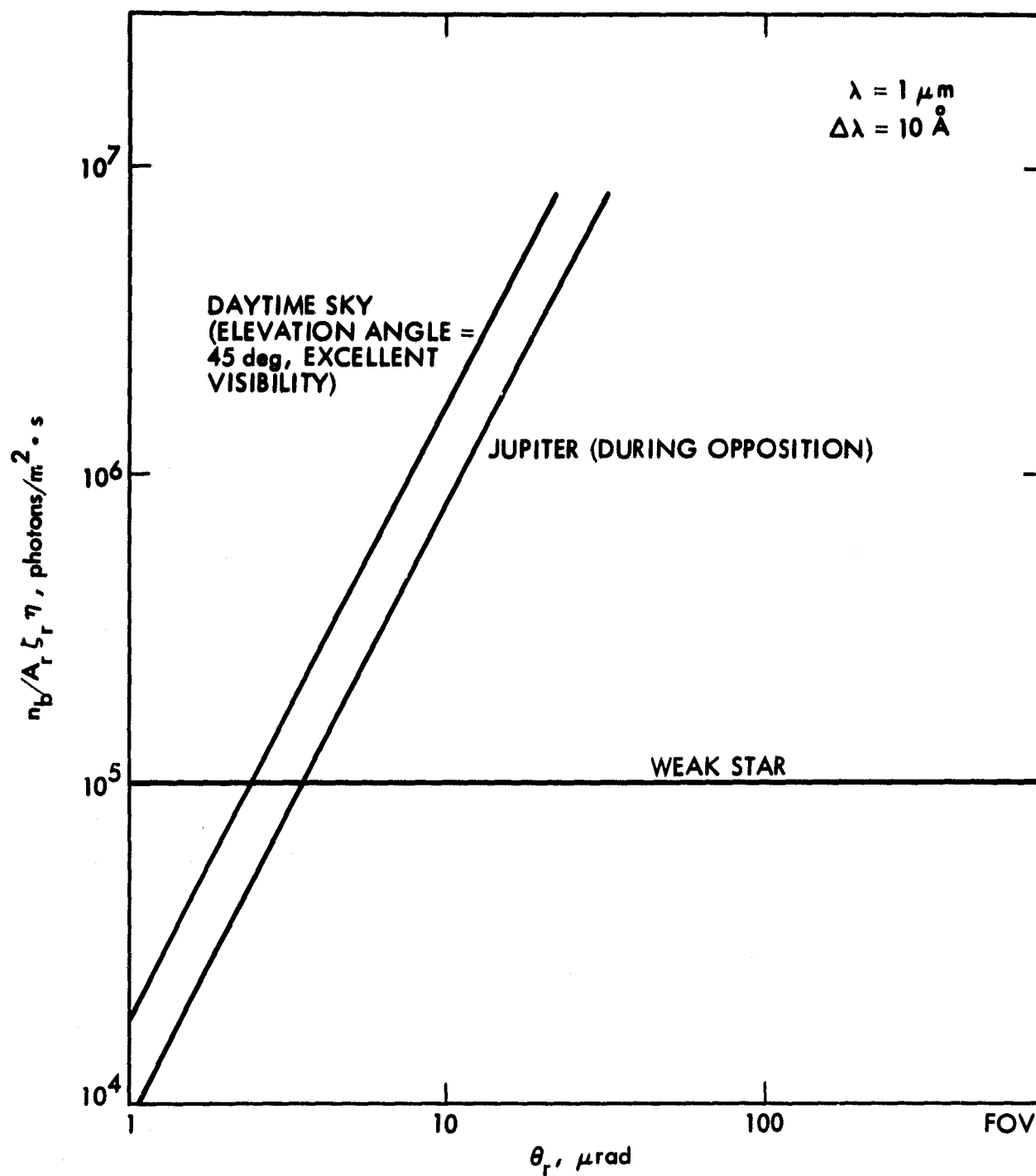
Figure B-1. Normalized Photon Rate as a Function of Receiver FOV for a Terrestrial Receiver
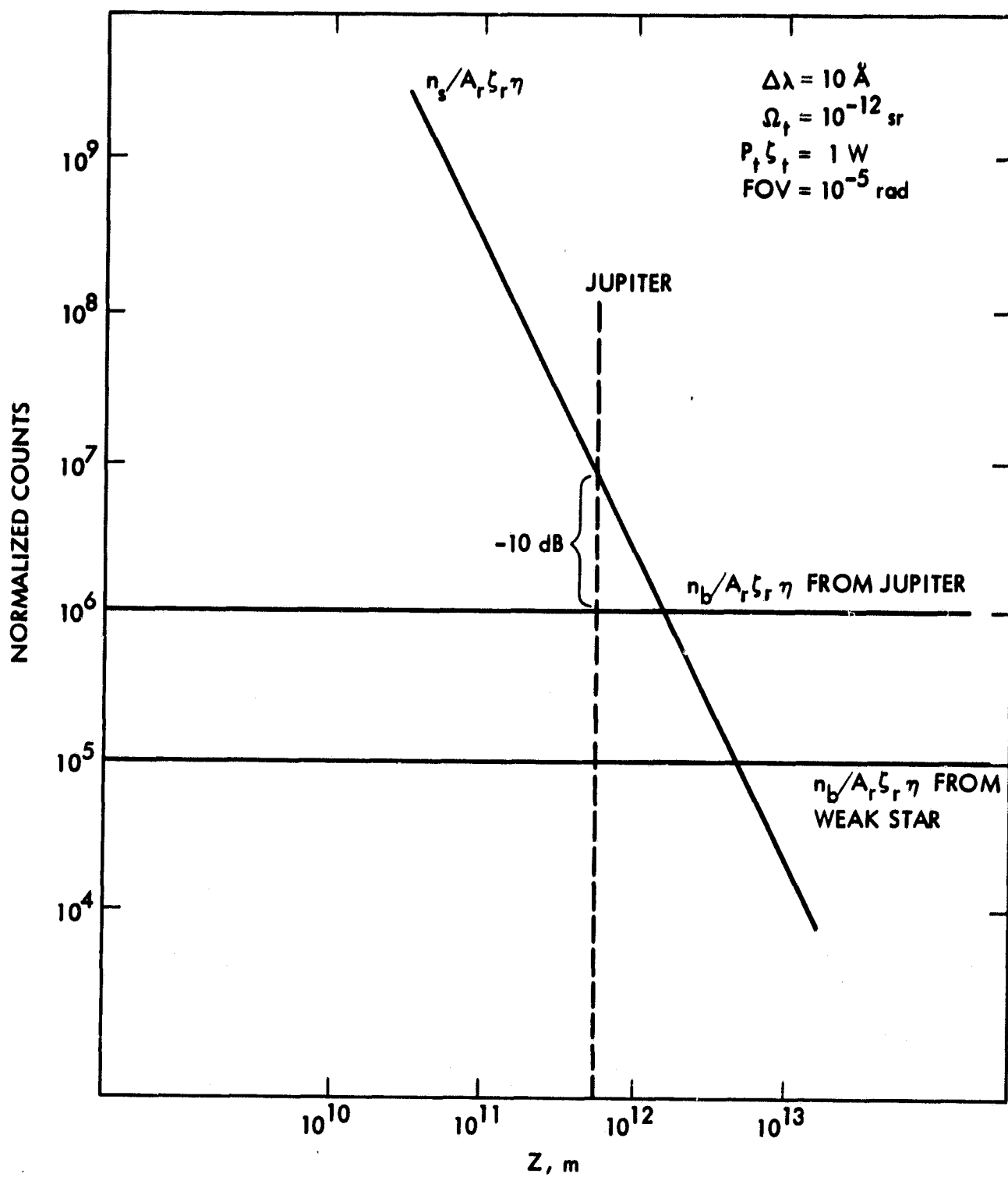
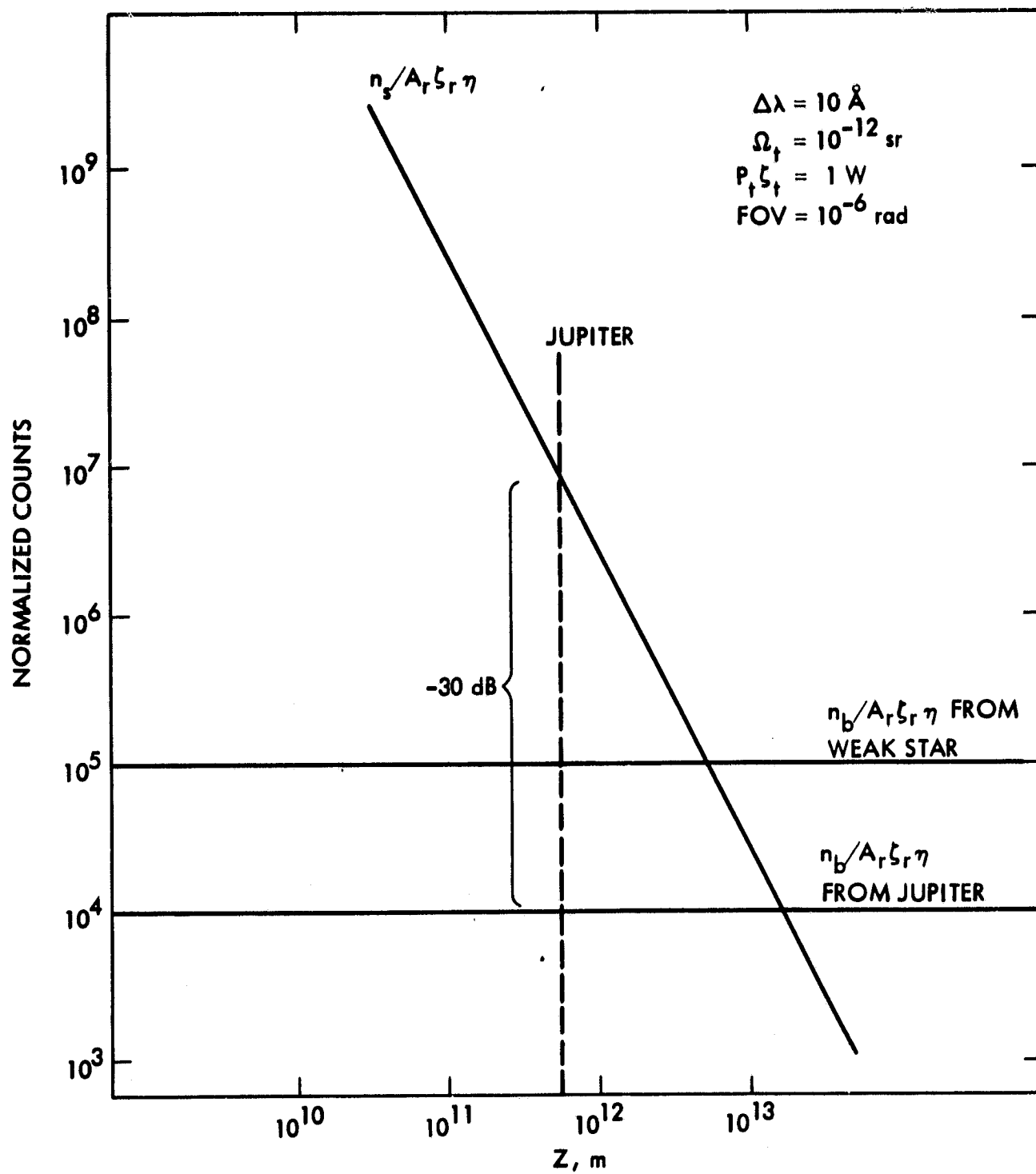Figure B-2. Comparison of Signal and Background Counts, FOV = 10 μrad

Figure B-3. Comparison of Signal and Background Counts, FOV = 1 μrad

deteriorates, resulting not only in reduced signal strength, but greater background noise power as well. One possible solution to this problem is to employ an optical receiver operating outside of the atmosphere, which is immune to background and visibility effects introduced by the Earth's atomsphere.